10

Interaction of Atom with Laser Pulses of Intra-Atomic Field Strength

A.V. Andreev, S.Yu. Stremoukhov and O.A.Shoutova
Physics Department, M.V. Lomonosov Moscow State University
Russia

1. Introduction

In spite of the twenty-year history, the effect of the high-order optical harmonic generation (HHG) is still under great interest of both experimentalists and theoreticians (see review (Ganeev, 2009)). The origin of this interest is manifold. From the practical point of view, the HHG is one of the effective mechanisms for producing coherent emission in broad range of electromagnetic wave spectrum. The plateau in the harmonic amplitude distribution in extreme ultraviolet (XUV) region affords grounds for development of subfemtosecond pulse formation methods (Paul, 2001). As a result, the new frontiers are opened up in science by extending the nonlinear optics and time-resolved spectroscopy to the XUV region (Papadogiannis, 2003) and pushing ultrafast science to the attosecond domain, enabling XUV spectroscopy and imaging of molecular orbitals (Itatani, 2004), surface dynamics (Tobey, 2007), and electron motion. Hence, the HHG effect opens up the new perspectives in attosecond science (Corkum, 2007; Sola, 2006).

At present days, the efficiency of conversion to high-order harmonics turns out to be insufficient for using them as real coherent short-wavelength radiation sources in biology, plasma diagnostics, medicine, microscopy, photolithography, etc. Hence, the search for ways of increasing the cut-off frequency and HHG efficiency in the XUV spectral range is still among the most topical problems of nonlinear optics.

The HHG effect was observed with the large number of periodic table elements having usually small and middle atomic numbers (Ganeev, 2009; 2005; 2007a;b; Redkin, 2010). As a rule, the interaction medium is gas jet, cell or laser plasma which is prepared by irradiation of metal surface by laser pre-pulse. The maximum harmonic order, or cut-off frequency (CF), obtained in plasma media to date varies from the sixties to seventies harmonics of fundamental frequency (Redkin, 2010; Suzuki, 2007). The highest-order harmonics (the 101st harmonic, λ =7,9 nm) have been obtained in manganese plasmas (Ganeev, 2007b). The efficiency of conversion in the plateau region amounts to $\sim 10^{-5}$ (Ganeev, 2007a). Recently, in experiments with silver plasma the CF values approximating seventies orders have been obtained (Ganeev, 2005). This value depends on both atomic levels structure and laser pulse parameters (intensity, energy and duration, envelope time-dependence, carrier-envelope phase). CF extension into higher frequencies band promises new possibilities in creating X-ray coherent sources and so the study of its behavior in dependence on media features and external laser pulse parameters is the problem of significant scientific and technical interest.

From the general point of view, it is clear that the emission spectrum is sensitive both to the spectral composition of the laser field and its polarization structure. At the beginning of

the 1990s, the method of two-pulse and two-frequency HHG spectrum control was proposed in (Watanabe, 1994; Yin, 1992), and the idea of polarization control was seemingly first introduced in (Corkum, 1994). Recently, it has been shown that the use of the two-color schemes, where two pulses with fundamental and double frequencies (ω and 2ω) interact simultaneously with atomic or molecular media, enable to enhance significantly the power of THz emission (Bartel, 2005; Cook, 2000; Kress, 2004) in comparison with the single pulse schemes (Hamster, 1994; 1993; Sprangle, 2004). In the latter case the ultrashort pulses of the high intensity are usually used. Earlier theories suggest the basic mechanism of THz emission is based on the four-wave-mixing rectification (FWMR) process in laser induced plasma (Gorbunov, 1996; Sprangle, 2004). This phenomenological models, formulated in terms of plasma nonlinear susceptibilities, have been also used to interpret the results of experiments based on the two-color schemes.

Up to now, there have been developed a number of different theoretical models to describe the dynamics of atomic electron motion in strong laser field. These models are based on different approximations, which are usually valid in the restricted area of laser pulse field strength. The intra-atomic field strength, $E_{at} = e/a_B^2$ (where a_B is the Bohr radius), is used as unit for measure of field strength. The approximations are different for subatomic, $E_0 \ll E_{at}$, and overatomic, $E_0 \gg E_{at}$, fields. The unified theory applicable for both weak and strong laser fields has not yet been developed. Indeed, let us make some short review of the proposed theoretical approaches. The foundation of the atom ionization theory has been laid by the paper of Keldysh (Keldysh, 1965). In the frame of this theory it is assumed that the atom has one bound state and the wave functions of continuum are calculated in quasiclassical approximation. The Keldysh theory has got further development in the series of papers (Perelomov, 1967a;b; Popov, 1968). The theory developed in these papers is known as the Perelomov–Popov–Terent'ev (PPT) model. Similar approach based on the calculation of the matrix element of the transition from the initial bound state of a system belonging to the discrete spectrum to the final state described by the Volkov wave function was developed in (Parker, 1990). The approach proposed in (Faisal, 1973; Keldysh, 1965; Reiss, 1980) is usually called the Keldysh–Faisal–Reiss (KFR) approximation. The model known as the strong-field approximation (SFA) was proposed and developed in the series of papers by Reiss (Reiss, 1990; 1992; 1980). In contrast to the Keldysh's theory, this approximation does not use the saddle point method in calculating the matrix element of the transition from initial atomic state to ionized state of the Volkov continuum and, hence, it does not need an assumption that the photon energy is much smaller than electron binding energy. The Kramers-Henneberger model developed in (Kulander, 1991; Marte, 1991; Pont, 1990) is the model of dressed atom, the ionization potential of which decreases with laser field strengthening.

Among others there is a method of direct numerical solution of time-dependent Schrödinger equation (TDSE). The first numerical calculations for the case of hydrogen atom have been done in (Krause, 1992). Later this approach was successfully applied in studies of the one- and multi-photon ionization of the different hydrogen-like atoms (see e.g. (Rae, 1994)) and during this time undergo certain improvement getting more and more sophisticated (Bauer, 2006; Muller, 1999). With rapid progress in computer technique there appeared a conception, that this method is the most effective one in studies of light-atom interactions at strong laser field regime, which could serve a criterion of rightness for other theoretical approaches. But this seems to be a delusion. There are some reasons for that. Firstly, any computer simulation inevitably deals with a modeled atom. To avoid the singularity of the Coulomb potential, some empirical approximations for intra-atomic potential are usually used (see e.g. (Volkova,

2006; 2001; 2007) and references therein). Secondly, it is usually supposed that the wave functions of the continuum spectrum states are the Volkov wavefunctions. However, in the limit of zero field strength these wave functions tend to the free particle wave functions but not to the wave functions of a particle in the Coulomb field. Thirdly, it has been shown that the gauge choice dramatically change the results of numerical solutions of TDSE down to obvious contradiction with other models (Bauer, 2005).

In the frame of above models, the harmonics of laser radiation frequency result from a three-stage process that comprises the ionization of an atom, the electron acceleration in the electromagnetic field, and the subsequent recombination with ion and emission of harmonics. This process is periodically repeated every half cycle of the electromagnetic wave. The evolution of the ionized electron is usually described with the help of Volkov wave functions or classical electrodynamics equations. Notice, that the use of the Volkov wave functions is due to the variation of the spatial profile of the atomic continuous spectrum eigenfunctions in the presence of external field. However, the spatial profile of the atomic discrete spectrum eigenfunctions is also changed in the presence of the external electromagnetic field. This is the principle inconsistence of the above methods, because the wave functions of discrete (hydrogenic) and continuous (Volkov) spectra, which are used as basis for TDSE wave function expansion, do not compose the complete basis of the orthogonal functions.

The alternative approach in the theory of light-atom interaction has been proposed in (Andreev, 1999). This approach is based on the exact mathematical solutions of the boundary value problem for electron moving in superposition of centro-symmetric intra-atomic field and field of external electromagnetic wave. In the non-relativistic approximation the spectrum of eigenvalues for this problem coincides with that for free atom boundary value problem and eigenfunctions $\varphi_n(\vec{r},t)$ are related by $\varphi_n(\vec{r},t) = u_n(\vec{r}) \exp\left(ie/\hbar c \vec{A}(t)\vec{r}\right)$ with the free atom eigenfuctions $u_n(\vec{r})$. The set of eigenfunctions $\varphi_n(\vec{r},t)$ provides the complete basis of the orthonormal functions which is used to calculate the matrix elements of quantum-mechanical operators. In the case of hydrogen-like atom or ion the dynamics of atomic electron over the states of both discrete and continuous spectra is calculated in consistent mathematical form. The main advantage of the proposed approach is its non-perturbative manner. The ratio of laser field strength E_0 to intra-atomic field strength $E_{at} = e/a_B^2$, where a_B is the Bohr radius, is not constrained by any conditions.

The paper is arranged as follows: Section 2 is devoted to the theory of eigensolutions of the boundary value problem for "atom in external field" and its applications to the general non-relativistic theory of light-atom interaction. The equations for atomic response are presented in Section 3. The results of computer simulations on the laser pulse interaction with silver atom are presented in Section 4. Finally, we summarize our findings in Section 5.

2. Basic principles of the theory

The traditional approach in the description of electromagnetic wave scattering by a single atom is based on the use of the eigenfunctions of free atom boundary value problem as the basis for wave function expansion. By solving the set of equations for probability amplitudes we can calculate the polarization of an ensemble of atoms. The polarization of atomic ensemble is the sum of the dipole moments of the individual atoms of ensemble. The eigenfunctions of the boundary value problem for an atom with the spherically symmetric intra-atomic potential have the following form

$$u_{nlm}(\vec{r}) = R_{nl}(r)\, Y_{lm}(\theta, \varphi), \tag{1}$$

where n is the principle quantum number, l and m are the angular momentum and its projection, respectively. The angular distribution of wave functions (1) possesses the spherical symmetry for the states with zero angular momentum and cylindrical symmetry for the states of non-zero angular momentum. Each state is characterized by the spatial parity $P = (-1)^l$. The matrix elements of dipole moment operator are defined by

$$\vec{d}_{nm} = e \langle n | \vec{r} | m \rangle. \tag{2}$$

Notice, that each of the states $|n\rangle$ is characterized by the three dimensional quantum number $n = (nlm)$. One can see from Eq.(2) that the dipole moment matrix elements take the non-zero values only for transitions between the states of opposite parity.

The angular dependency of the wave functions (1) is specified in the coordinate set of the individual atom configurational space. Indeed, the quantum mechanical average of the angular momentum in the states (1) reads as

$$\langle nlm | \vec{l} | nlm \rangle = \vec{n}_z \hbar m. \tag{3}$$

So, the direction of axis z in configurational space coincides with the direction of the average angular momentum of any individual atom. Under calculation of the matrix elements (2) it is usually assumed that the polarization vector of the linearly polarized wave is parallel to the axis z, i.e. $\vec{e}^{(0)} = \vec{n}_z$, and polarization vectors of circularly polarized wave lie in the perpendicular plane, i.e. $\vec{e}^{(\pm)} = \left(\vec{n}_x \pm \vec{n}_y\right)/\sqrt{2}$.

By expanding the wave functions of the time dependent Schrodinger equation (TDSE) into the series of eigenfunctions (1)

$$\psi(\vec{r}, t) = \sum_n a_n(t)\, u_n(\vec{r}) \tag{4}$$

and making summation over the physically small volume V_1, for the polarization of atomic ensemble we get

$$\vec{P}(\vec{r}_0, t) = \sum_{i \in V_1} \sum_{n,m} a_n^{(i)*}(t)\, a_m^{(i)}(t)\, \vec{d}_{nm}^{(i)}, \tag{5}$$

where $\vec{r}_0$ is the center-of-mass coordinate of the physically small volume V_1, and i is the summation index over the atoms located in this volume.

By summarizing the short sketch of the traditional methods based on the TDSE wave function expansion into the series of the free atom eigenfunctions we can conclude. Firstly, the atomic response is observed only in the process of inelastic electromagnetic wave scattering. Indeed, the matrix elements (2) have non-zero values only in the case when the initial and final states of transition have the opposite parity. As far as the eigenvalues corresponding to the eigenfunctions (1) depend on the angular momentum, l, hence, the atomic electron energies in the initial and final states of transitions are different. Secondly, the directions of dipole moments of all atoms in ensemble coincide. Indeed, the assumption on $\vec{e}^{(0)} \parallel \vec{n}_z^{(i)}$ and $\vec{e}^{(\pm)} \perp \vec{n}_z^{(i)}$ leads unambiguously to the following relationship $\vec{d}_{nm}^{(i)} = \vec{d}_{nm}$.

However, both these conclusions are in contradiction with the results of experimental measurements. Firstly, the dielectric permittivity of atomic gases does not equal unity even in spectral region of frequencies which are a few orders of magnitudes smaller than the

frequency of the nearest dipole allowed transition. In this case the population of the excited atomic states is negligibly small, and the atomic response is mainly due to the processes of electromagnetic wave elastic scattering. Secondly, the direction of electromagnetic wave polarization vector is strongly fixed at any spatial point of atomic ensemble. At the same time, the angular moments of different atoms of ensemble are chaotically directed. Hence, the assumption on $\left\langle \vec{l}_i \right\rangle \parallel \vec{e}$ could not be valid in principle.

Here we develop the theory of light-atom interaction, which is free of the above contradictions. The most principle innovation of the proposed theory is in the fact that the basis of eigenfunctions of the boundary value problem for "atom in the external field" is used to calculate the matrix elements of quantum mechanical operators. It was shown in (Andreev, 2010) that the bases of the "free atom" $u_n(\vec{r})$ and "atom in the external field" $\varphi_n(\vec{r},t)$ eigenfunctions are related by $\varphi_n(\vec{r},t) = u_n(\vec{r}) \exp\left[i\left(q/\hbar c\right)\vec{A}(t)\,\vec{r}\right]$. Each basis is the complete set of orthonormal functions, hence, any eigenfunction of any basis can be expanded into series of another basis eigenfunctions. For example, $u_n(\vec{r}) = \sum\limits_m V_{nm}\varphi_m(\vec{r},t)$. By substituting this expansion into (4) we get for some individual atom

$$\vec{P}(t) = \sum_{n,m,p,q} a_n^*(t)\, a_m(t)\, V_{np}^{-1}(t)\, \vec{d}_{pq} V_{qm}(t). \tag{6}$$

By comparing the Eqs. (5) and (6) one can see the following principle difference between these equations. Firstly, the dipole moment matrix elements became time dependent

$$\vec{d}_{nm}(t) = \sum_{p,q} V_{np}^{-1}(t)\, \vec{d}_{pq} V_{qm}(t).$$

It is seen that the matrix elements $V_{nm}(t)$ play the crucial role in the frames of the developed approach. These matrix elements are the nonlinear functions of the electromagnetic field strength and they determine the temporal evolution of matrix elements of quantum mechanical operators. Secondly, and this is the most principle, the atomic polarization is time dependable even in the case when atom is in the ground state during the whole process of light-atom interaction. Indeed, let the state $n = 0$ be the ground atomic state. Assuming in (6) $a_n(t) = \delta_{n0}$ we get

$$\vec{P}_0(t) = \sum_{p,q} V_{0p}^{-1}(t)\, \vec{d}_{pq} V_{q0}(t).$$

Thus we can see that an atom, being the whole time in the ground state, produces the response, the spectrum of which depends on temporal evolution of matrix elements $V_{nm}(t)$.

2.1 Boundary value problem for an atom in the external field

The boundary value problem for an atom with a spherically symmetric potential has the form

$$\left[\frac{\vec{p}^2}{2m} + U(r)\right] u_n(\vec{r}) = E_n u_n(\vec{r}). \tag{7}$$

Despite the explicit form of the spherical interatomic potential, the eigenfunction of this problem can be written as

$$u_{nlm}(\vec{r}) = R_{nl}(r)\, Y_{lm}(\theta,\varphi), \tag{8}$$

where $Y_{lm}(\theta,\varphi)$ are spherical functions and $R_{nl}(r)$ are radial functions determined by the given boundary conditions at $r=0$ and $r=\infty$.
Now we turn to the boundary value problem for an atom in the external field. Restricting our frames to the nonrelativistic approximation and taking $\vec{A}(\vec{r},t) \approx \vec{A}(t)$, we obtain the boundary value problem:

$$\left[\frac{1}{2m}\left(\vec{p}-\frac{q}{c}\vec{A}(t)\right)^2+U(r)\right]\varphi_N(\vec{r},t)=E_N\varphi_N(\vec{r},t). \tag{9}$$

Substituting the wavefunction

$$\varphi_N(\vec{r},t)=u_n(\vec{r})\exp\left(i\frac{q}{\hbar c}\vec{A}(t)\vec{r}\right) \tag{10}$$

into (4), we obtain an expression duplicating (7), where

$$E_N=E_n. \tag{11}$$

Hence, we should conclude that the eigenvalues of the two problems (7) and (9) explicitly coincide and the eigenfunctions differ. As mentioned above, quantum number n represents a set of three quantum numbers $n=(nlm)$, which uniquely define the angular and radial functions within the $u_{nlm}(\vec{r})$. Due to the simplicity of expression (10), it is reasonable to put $N=(nlm)$. However, note that the angular and radial parts of wavefunctions $\varphi_N(\vec{r},t)$ are, in the general case, time-dependent features and therefore (nlm) no longer have the sense of quantum numbers, which are per se conservative values. Note that $|\varphi_N(\vec{r},t)|^2=|u_n(\vec{r})|^2$, which means that the spatial distribution of probability does not change. This means that the energy of Coulomb interaction between the electron and atomic nucleus does not vary. Furthermore, the same can be stated about all spatial moments: $P_\alpha^{(nm)}=\int u_n^* x_\alpha u_m dV=\int \varphi_n^* x_\alpha \varphi_m dV$, $P_{\alpha\beta}^{(nm)}=\int u_n^* x_\alpha x_\beta u_m dV=\int \varphi_n^* x_\alpha x_\beta \varphi_m dV$, etc. This lies at the base of the equality of eigenvalues (11).

2.2 Relation between two sets of eigenfunctions

Set of functions $\varphi_n(\vec{r},t)$ also forms the complete orthonormal basis as the set $u_n(\vec{r})$. The orthonormality and completeness conditions for functions $\varphi_n(\vec{r},t)$ are

$$\begin{gathered}\int \varphi_n^*(\vec{r},t)\,\varphi_m(\vec{r},t)\,dV=\int u_n^*(\vec{r})\,u_m(\vec{r})\,dV=\delta_{nm}\\ \sum_n \varphi_n^*(\vec{r},t)\,\varphi_n(\vec{r}',t)=\exp\left[-i\frac{q}{\hbar c}\vec{A}(t)(\vec{r}-\vec{r}')\right]\sum_n u_n^*(\vec{r})\,u_n(\vec{r}')=\delta(\vec{r}-\vec{r}').\end{gathered} \tag{12}$$

Therefore, any function from one set can be represented as an expansion into series of eigenfunctions of the other:

$$\varphi_n(\vec{r},t)=\sum_m V_{nm}^{-1}u_m(\vec{r}),\quad u_n(\vec{r})=\sum_m V_{nm}\varphi_m(\vec{r},t), \tag{13}$$

where transformation operator V, according to (10), takes the form

$$V=\exp\left(-i\frac{q}{\hbar c}\vec{A}(t)\vec{r}\right). \tag{14}$$

Introducing the three-dimensional form of indexes, we can rewrite (13) as

$$\varphi_{n_1l_1m_1}(\vec{r},t)=\sum_{n_2l_2m_2}\langle n_2l_2m_2|\,V^{-1}\,|n_1l_1m_1\rangle\,u_{n_2l_2m_2}(\vec{r}). \tag{15}$$

Using the well-known expansion for the exponent,

$$\exp\left(i\frac{q}{\hbar c}\vec{A}(t)\vec{r}\right)=4\pi\sum_{l=0}^{\infty}\sum_{m=-l}^{l}i^{l}j_{l}\left(\frac{q}{\hbar c}A(t)r\right)Y_{lm}^{*}\left(\vec{e}(t)\right)Y_{lm}\left(\vec{n}\right), \tag{16}$$

where $\vec{e}(t)=\vec{A}(t)/A(t)$ and $j_l(z)$ are spherical Bessel functions, for matrix elements on RHS of(15), we obtain the following expression:

$$\left\langle n_2l_2m_2\right|V^{-1}\left|n_1l_1m_1\right\rangle=4\pi\sum_{l=0}^{\infty}i^{l}\int_{0}^{\infty}R_{n_2l_2}(r)\,j_{l}\left(\frac{q}{\hbar c}A(t)r\right)R_{n_1l_1}(r)\,r^{2}dr\cdot$$
$$\cdot\sum_{m=-l}^{l}Y_{lm}^{*}\left(\vec{e}(t)\right)\int Y_{l_2m_2}^{*}(\theta,\varphi)\,Y_{lm}(\theta,\varphi)\,Y_{l_1m_1}(\theta,\varphi)\,do,$$

where $do=\sin\theta d\theta d\varphi$. Integration over angular variables can be performed analytically:

$$\int Y_{l_2m_2}^{*}(\theta,\varphi)\,Y_{lm}(\theta,\varphi)\,Y_{l_1m_1}(\theta,\varphi)\,do=$$
$$=(-1)^{m_2}\,i^{-l_2+l_1+l}\begin{pmatrix}l_2 & l & l_1\\ -m_2 & m & m_1\end{pmatrix}\begin{pmatrix}l_2 & l & l_1\\ 0 & 0 & 0\end{pmatrix}\cdot\sqrt{\tfrac{(2l+1)(2l_1+1)(2l_2+1)}{4\pi}} \tag{17}$$

so, the matrix element is modified as follows:

$$\left\langle n_2l_2m_2\right|V^{-1}\left|n_1l_1m_1\right\rangle=\sum_{l=|l_1-l_2|}^{l_1+l_2}Y_{lm}^{*}\left(\vec{e}(t)\right)C\left(lm\,|l_2m_2,l_1m_1\right)\left\langle n_2l_2\left\|j_{l}\left(\frac{q}{\hbar c}A(t)r\right)\right\|n_1l_1\right\rangle, \tag{18}$$

where we have introduced the coefficients $C\left(lm\,|l_2m_2,l_1m_1\right)$ in the way seen from comparison (17) and (18) and the reduced radial matrix elements are

$$\left\langle n_2l_2\left\|j_{l}\left(\frac{q}{\hbar c}A(t)r\right)\right\|n_1l_1\right\rangle=\int_{0}^{\infty}R_{n_2l_2}(r)\,j_{l}\left(\frac{q}{\hbar c}A(t)r\right)R_{n_1l_1}(r)\,r^{2}dr. \tag{19}$$

Hence, the angular part of matrix elements V_{nm} is calculated analytically. The radial part can also be calculated in analytic form if we choose the set of hydrogenic eigenfunctions, which is only, known up to date, complete of three - dimensional boundary value problem.
Substituting (18) into (15), we finally obtain

$$\varphi_{n_1l_1m_1}(\vec{r},t)=\sum_{n_2l_2m_2}\sum_{l=|l_1-l_2|}^{l_1+l_2}R_{n_2l_2}(r)\left\langle n_2l_2\left\|j_{l}\right\|n_1l_1\right\rangle Y_{lm}^{*}\left(\vec{e}\right)Y_{l_2m_2}\left(\vec{n}\right)\cdot C\left(lm\,|l_2m_2,l_1m_1\right). \tag{20}$$

This expression reveals that the angular part of $\varphi_n(\vec{r},t)$ depends on both the electric field direction $\vec{e}$ and on the angular momentum of the atom $\langle\vec{l}\rangle$.
Wavefunctions $\varphi_n(\vec{r},t)$ take the form of axially symmetric function in two cases: (1) $l_1=0$, (2) $\vec{e}\parallel\vec{n}_z$.
In the first case, wavefunction (15) takes the form

$$\varphi_{n_1l_1=0}(\vec{r},t)=2\sqrt{\pi}\sum_{n_2l_2}(-1)^{l_2}R_{n_2l_2}(r)\left\langle n_2l_2\left\|j_{l_2}\right\|n_10\right\rangle\sum_{m_2=-l_2}^{l_2}Y_{l_2m_2}^{*}\left(\vec{e}\right)Y_{l_2m_2}\left(\vec{n}\right), \tag{21}$$

and if we use the relation

$$\sum_{m=-l}^{l}Y_{lm}^{*}\left(\vec{e}\right)Y_{lm}\left(\vec{n}\right)=\frac{2l+1}{4\pi}P_{l}\left(\vec{e}\vec{n}\right),$$

we would see that function (15) is axially symmetric with the axis of symmetry, which coincides with the external electric field polarization.
In the second case, due to the relation

$$Y_{lm}\left(\vec{e}\right)|_{\vec{e}=\vec{n}_z} = i^l\sqrt{\frac{2l+1}{4\pi}}\delta_{m0},$$

we obtain

$$\varphi_{n_1 l_1 m_1}\left(\vec{r},t\right) = \sum_{n_2 l_2}\sum_{l=|l_1-l_2|}^{l_1+l_2} i^l\sqrt{\tfrac{2l+1}{4\pi}}R_{n_2 l_2}\left(r\right)\left\langle n_2 l_2 \left\| j_l \right\| n_1 l_1\right\rangle Y_{l_2 m_1}\left(\vec{n}\right) C\left(l0\left|l_2 m_1, l_1 m_1\right.\right). \quad (22)$$

Note, that wavefunction (15) is the superposition of wavefunctions $u_{n'l'm}\left(\vec{r}\right)$ with an identical value of the angular momentum projection on the external field direction. This testifies to the fact that only the angular momentum projection is a conservative value of problem (9) and the angular momentum itself is not.

2.3 Equations for the probability amplitudes

In the subrelativistic region of the electromagnetic field, the laser pulse interaction with a single atom is governed by the time-dependent Schrodinger equation (TDSE)

$$i\hbar\frac{\partial\psi}{\partial t} = \left[\frac{1}{2m}\left(\vec{p}-\frac{q}{c}\vec{A}\left(t\right)\right)^2 + U\left(r\right)\right]\psi. \quad (23)$$

The Hamiltonian matrix elements within sets of eigenfunctions (8) and (10) are, respectively,

$$\begin{gathered}\int u_n^*\left(\vec{r}\right)\left[\tfrac{1}{2m}\left(\vec{p}-\tfrac{q}{c}\vec{A}\right)^2 + U\left(r\right)\right]u_m\left(\vec{r}\right)dV = \sum_p V_{np}^{-1}\left(t\right)E_p V_{pm}\left(t\right),\\ \int \varphi_n^*\left(\vec{r},t\right)\left[\tfrac{1}{2m}\left(\vec{p}-\tfrac{q}{c}\vec{A}\right)^2 + U\left(r\right)\right]\varphi_m\left(\vec{r},t\right)dV = E_n\delta_{nm}.\end{gathered} \quad (24)$$

We see that the matrix elements within the set of eigenfunctions $\varphi_n\left(\vec{r},t\right)$ have rather plain structure, since they are the eigenfunctions of the Hamiltonian of Eq. (23). So, at first glance, we should find it more reasonable to expand the wavefunction of the TDSE into series of eigenfunctions of the boundary value problem (9). However, the presence of the time derivative on the left-hand side of Eq. (23) forces us to deal with the integral $\int \varphi_n^*\left(\vec{r},t\right)\partial\varphi_m\left(\vec{r},t\right)/\partial t dV$. And since the Hamiltonian of problem (9) is time-dependent, derivatives $\partial\varphi_n\left(\vec{r},t\right)/\partial t$ cannot be eigenfunctions of problem (9) and are therefore not orthogonal to functions φ_n.
At the same time, as mentioned above, the eigenfunctions of the problems (7) and (9) are related to each other in a simple way, so, we can expand wavefunction of the TDSE into series of free atom eigenfunctions

$$\psi\left(\vec{r},t\right) = \sum_n a_n\left(t\right)u_n\left(\vec{r}\right), \quad (25)$$

and then use the relation equation (13). Omitting some evident details, for the probability amplitudes $a_n\left(t\right)$ we can get the following set of equations

$$i\hbar\frac{da_n}{dt} = \sum_{m,k} V_{nk}^{-1}E_k V_{km}a_m. \quad (26)$$

We see that the matrix elements of operator V play the very important in the frame of developed theory. We now introduce the compound matrix elements:

$$M_{nm} = \sum_k V_{nk}^{-1} E_k V_{km}. \tag{27}$$

According to definition (14), operator V can be represented as an infinite series of the vector potential powers. If we restrict our consideration by the linear terms only, then in the weak field approximation we get

$$M_{nm} \approx \sum_k \left(1 + i\frac{q}{\hbar c}\vec{A}\vec{r} + \cdots\right)_{nk} E_k \left(1 - i\frac{q}{\hbar c}\vec{A}\vec{r} + \cdots\right)_{km}. \tag{28}$$

Retaining on the right-hand side only linear field terms, we obtain:

$$M_{nm} = E_n\delta_{nm} - i\omega_{nm}\frac{q}{c}\left(\vec{A}\vec{r}\right)_{nm} + \cdots.$$

In the case of $\vec{A}(t) = \vec{A}_0 \exp(-i\omega_0 t)$ and $\omega_0 \approx \omega_{nm}$, the relation between the field strength and the vector potential is

$$\vec{E}(t) = -\frac{1}{c}\frac{\partial\vec{A}}{\partial t} = \frac{i\omega_0}{c}\vec{A} \approx \frac{i\omega_{nm}}{c}\vec{A}.$$

Finally, for the compound matrix elements in the weak field approximation we get

$$M_{nm} \approx E_n\delta_{nm} - q\left(\vec{E}\vec{r}\right)_{nm} + \cdots.$$

So, one can see, that in the weak field approximation the set of equations (26) transforms to the set of equations for a two-level atom interacting with the field within the resonant electro–dipole approximation. Therefore, Eqs. (26) include not only resonant electro–dipole interaction (i.e. without the assumption $\omega_0 \approx \omega_{nm}$), but the non-resonant electro–dipole interaction, as well as interactions of higher multipolarity order, which originates from the terms in Eq. (27) with higher field power.

2.4 Basic peculiarities of the proposed theory

The general expression for the matrix elements V_{nm} is given by (18). Nevertheless, let us make some simple examples. These matrix elements have the most compact and simplest form when one of the states is $|ns\rangle$ state:

$$\langle ns|\, V^{-1}\, |n's\rangle = \langle ns\,\|j_0(z)\|\, n's\rangle, \tag{29}$$

$$\langle ns|\, V^{-1}\, |n'pm\rangle = i\sqrt{4\pi}\,\langle ns\,\|j_1(z)\|\, n'p\rangle\, Y_{1m}(\vec{e}), \tag{30}$$

$$\langle ns|\, V^{-1}\, |n'dm\rangle = -\sqrt{4\pi}\,\langle ns\,\|j_2(z)\|\, n'd\rangle\, Y_{2m}(\vec{e}). \tag{31}$$

where $z = \frac{q}{\hbar c}A(t)\,r$. In this case the dependency of matrix elements on the electromagnetic wave polarization vector is described by the spherical harmonics. The dependency on the field amplitude is associated with the reduced matrix elements $\langle n_2 l_2\,\|j_l(z)\|\, n_1 l_1\rangle$. As we

have mentioned above, in the case of hydrogenic wave functions the reduced matrix elements are calculated in the explicit analytic form. For example,

$$\langle 1s|\, j_0\, |1s\rangle = \frac{16}{(4+\mu^2)^2}, \quad \langle 2s|\, j_0\, |2s\rangle = \frac{1-3\mu^2+2\mu^4}{(1+\mu^2)^4},$$
$$\langle 2p, m=1|\, j_0\, |2p, m=1\rangle = \frac{1}{(1+\mu^2)^3}, \quad \langle 2p, m=0|\, j_0\, |2p, m=0\rangle = \frac{1-5\mu^2}{(1+\mu^2)^4},$$

$$\langle 1s|\, j_0\, |2s\rangle = \frac{256\sqrt{2}\mu^2}{(9+4\mu^2)^3}, \quad \langle 1s|\, j_1\, |2p\rangle = \frac{384\sqrt{2}\mu}{(9+4\mu^2)^3}, \quad \langle 1s|\, j_2\, |3d\rangle = \frac{6912\sqrt{6}\mu^2}{(16+9\mu^2)^4},$$

where

$$\mu(t) = \frac{qA(t)\, a_B}{\hbar c},$$

and a_B is the Bohr radius. By introducing the vector potential amplitude A_0, it is convenient to define the problem control parameter as follows

$$\mu_0 = \frac{qA_0 a_B}{\hbar c} = \frac{eE_0 a_B}{\hbar\omega} = \frac{2U_0}{\hbar\omega}\frac{E_0}{E_{at}}, \tag{32}$$

where $U_0 = Ry$ is the hydrogen atom ionization energy and $E_{at} = e/a_B^2$ is the strength of intra-atomic field.

It is seen that in the case of the hydrogen atom the parameter μ_0 is explicitly related with the adiabatic parameter of the Keldysh's ionization theory (Keldysh, 1965)

$$\gamma = \frac{\omega\sqrt{2mU_0}}{eE_0}.$$

Indeed, for the case of the hydrogen atom the parameter γ reads

$$\gamma = \frac{me\omega}{\hbar E_0} = \frac{\hbar\omega}{eE_0 a_B}.$$

Thus, the parameters μ_0 and γ are related by

$$\mu_0\gamma = 1.$$

Some reduced matrix elements for discrete – discrete transitions are shown graphically in Fig. 1a. The presented curves illustrate the main properties of these matrix elements. The diagonal matrix elements $\langle nl\,\|j_0\|\,nl\rangle$ tend to unity at $\mu \to 0$, which is due to the eigenfunction normalization condition. The asymptotical behavior of the matrix elements at $\mu_0 << 1$ can be obtained from the asymptotical expansion of the Bessel function

$$\begin{aligned}\langle n_2 l_2\,\|j_l(\mu(t)\rho)\|\,n_1 l_1\rangle = \mu^l \frac{\Gamma(1/2)}{2^{l+1}\Gamma(l+3/2)}\int_0^\infty R_{n_2 l_2}(\rho)\, R_{n_1 l_1}(\rho)\,\rho^{l+2}d\rho - \\ -\mu^{l+2}\frac{\Gamma(1/2)}{2^{l+3}\Gamma(l+5/2)}\int_0^\infty R_{n_2 l_2}(\rho)\, R_{n_1 l_1}(\rho)\,\rho^{l+4}d\rho + \cdots,\end{aligned} \tag{33}$$

where $\rho = r/a_B$. In accordance with the Wigner $3j$ symbol properties there are the following constraints: $|l_2 - l_1| \leqslant l \leqslant l_2 + l_1$. As a result, in the case of weak fields the matrix elements have the following asymptotics $\langle n_2 l_2\,\|j_l\|\,n_1 l_1\rangle \sim \mu^{|l_2-l_1|}$. On the other hand, in the region of the overatomic field strength, i.e. $\mu_0 >> 1$, the Bessel functions have the following

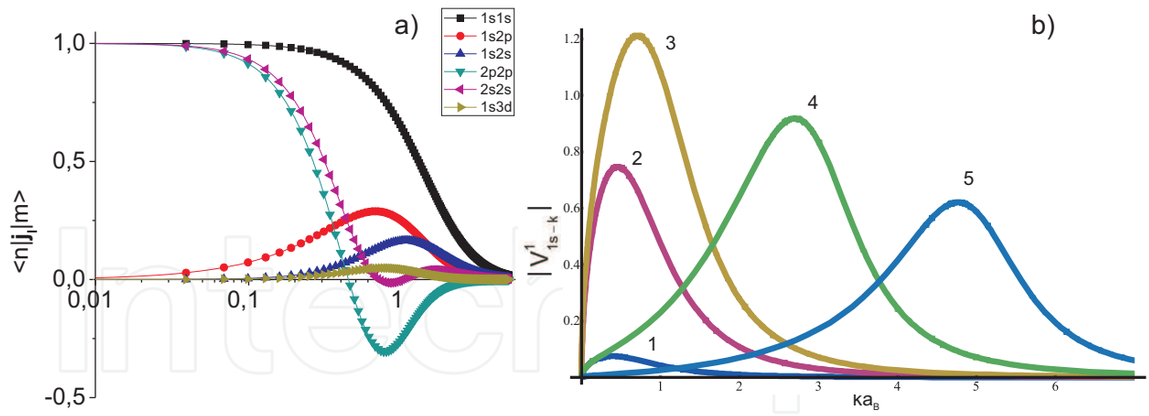

Fig. 1. Matrix elements for (a) discret-discret transitions as function of field strength, μ_0, and (b) discret-continuum transitions as function of photoelectron wave number, ka_B:
1. $V_{1s-k}(\mu_0 = 0.05, k)$, 2. $V_{1s-k}(\mu_0 = 0.5, k)$, 3. $V_{1s-k}(\mu_0 = 1, k)$, 4. $V_{1s-k}(\mu_0 = 3, k)$,
5. $V_{1s-k}(\mu_0 = 5, k)$

asymptotical behavior $j_l(\mu\rho) \approx \sin\left(\mu\rho - \frac{\pi l}{2}\right)/\mu\rho$. Hence, the matrix elements decrease with the field strength. Such behavior can be seen from Fig. 1a.
The matrix elements as function of photoelectron wave number for some discrete – continuum transitions are shown in Fig. 1b. One can see that the energy width of the populated continuum states increases with the increase of laser field strength.
Let us compare the common and distinctive features of equations (26) and equations for the probability amplitudes which follow from TDSE in electro-dipole approximation

$$i\hbar\frac{da_n}{dt} = \sum_m \left(E_n\delta_{nm} - \vec{E}\vec{d}_{nm}\right)a_m, \tag{34}$$

where E_n are the eigenvalues of the boundary value problem (7), δ_{nm} is the Kronecker delta function, and $\vec{d}_{nm}$ are the matrix elements of dipole moment operator. The most principle difference between the equations (26) and equations (34) is in the following.
It is seen that the diagonal elements of equations (34) coincide with the eigenvalues for "free atom" boundary value problem (7). At the same time, the diagonal elements of the Eq.(26) depend on the instantaneous laser field amplitude, because they are

$$M_{nn}(t) = \sum_k V_{nk}^{-1}(t)\, E_k V_{kn}(t). \tag{35}$$

Taking into account the above mentioned properties of the matrix elements V_{nm} it is seen that the diagonal elements (35) depend on the laser field amplitude. This dependency is due to the shifts of the effective energy of atom which in the presence of the external field is still in the "free atom" state (8). However, by comparing equations (8) and (10) we can see that state (8) is not an eigenstate of atom in the external field. Hence, its energy should depend on the field amplitude, and Eq.(35) describes the energy shifts, which are usually associated with the Stark shift, quadrupole splitting, etc. For the diagonal compound matrix elements $\langle nlm|M|nlm\rangle$ in the case of $|ns\rangle$ states we get

$$\langle ns|M|ns\rangle = \sum_{n'}\left[E_{n's}\left|\langle ns\|j_0(z)\|n's\rangle\right|^2 + 3E_{n'p}\left|\langle ns\|j_1(z)\|n'p\rangle\right|^2 + 5E_{n'd}\left|\langle ns\|j_2(z)\|n'd\rangle\right|^2\right]. \tag{36}$$

One can easily guess that the coefficients 3 and 5 appear due to the intermediate summation over the angular momentum projections of $|np\rangle$ and $|nd\rangle$ states. The diagonal matrix elements of $|npm\rangle$ states with $m = 0$ are

$$\begin{gathered}\langle npm|\, M\,|npm\rangle|_{m=0} = \sum_{n'}\Big\{3E_{n's}\,\langle np\,\|j_1(z)\|\,n's\rangle^2\cos^2\theta + \\ +\tfrac{E_{n'p}}{2}\Big[2\,\langle np\,\|j_0(z)\|\,n'p\rangle^2 + 2\,\langle np\,\|j_0(z)\|\,n'p\rangle\,\langle n'p\,\|j_2(z)\|\,np\rangle + 5\,\langle np\,\|j_0(z)\|\,n'p\rangle^2 + \\ +3\,\langle np\,\|j_2(z)\|\,n'p\rangle\,(2\,\langle n'p\,\|j_0(z)\|\,np\rangle + \langle n'p\,\|j_2(z)\|\,np\rangle)\cos 2\theta\Big] + \\ +\tfrac{3E_{n'd}}{10}\Big[7\,\langle np\,\|j_1(z)\|\,n'd\rangle^2 + 6\,\langle np\,\|j_1(z)\|\,n'd\rangle\,\langle n'd\,\|j_3(z)\|\,np\rangle + 12\,\langle np\,\|j_3(z)\|\,n'd\rangle^2 + \\ +\Big(\langle np\,\|j_1(z)\|\,n'd\rangle^2 + 18\,\langle np\,\|j_1(z)\|\,n'd\rangle\,\langle n'd\,\|j_3(z)\|\,np\rangle + 6\,\langle np\,\|j_3(z)\|\,n'd\rangle^2\Big)\cos 2\theta\Big]\Big\}\end{gathered} \tag{37}$$

where $\theta = \arccos(\vec{n}_z\vec{e})$. In the case of $m = \pm 1$ the matrix elements are

$$\begin{gathered}\langle npm|\, M\,|npm\rangle|_{m=\pm1} = \sum_{n'}\Big\{\tfrac{3}{2}E_{n's}\,\langle np\,\|j_1(z)\|\,n's\rangle^2\sin^2\theta + \\ +\tfrac{E_{n'p}}{4}\Big[4\,\langle np\,\|j_0(z)\|\,n'p\rangle^2 - 2\,\langle np\,\|j_0(z)\|\,n'p\rangle\,\langle n'p\,\|j_2(z)\|\,np\rangle + 7\,\langle np\,\|j_0(z)\|\,n'p\rangle^2 - \\ -3\,\langle np\,\|j_2(z)\|\,n'p\rangle\,(2\,\langle n'p\,\|j_0(z)\|\,np\rangle + \langle n'p\,\|j_2(z)\|\,np\rangle)\cos 2\theta\Big] - \\ -\tfrac{3E_{n'd}}{10}\Big[-13\,\langle np\,\|j_1(z)\|\,n'd\rangle^2 + 6\,\langle np\,\|j_1(z)\|\,n'd\rangle\,\langle n'd\,\|j_3(z)\|\,np\rangle - 18\,\langle np\,\|j_3(z)\|\,n'd\rangle^2 + \\ +\Big(\langle np\,\|j_1(z)\|\,n'd\rangle^2 + 18\,\langle np\,\|j_1(z)\|\,n'd\rangle\,\langle n'd\,\|j_3(z)\|\,np\rangle + 6\,\langle np\,\|j_3(z)\|\,n'd\rangle^2\Big)\cos 2\theta\Big]\Big\}\end{gathered} \tag{38}$$

One can see from Eqs. (36) - (38) that the effective energies of states are the non-linear functions of laser field strength, which can be expanded into the infinite series of the even powers of field. The effective energies of $|ns\rangle$ states do not depend on the orientation of the electromagnetic field polarization vector. It is quite evident because the spatial distribution of wave functions of $|ns\rangle$ states is spherically symmetric. At the same time the effective energies of $|npm\rangle$ states depend on the polarization vector orientation, because the wave function spatial distribution for the states with $l > 0$ possesses only cylindrical symmetry with respect to direction of angular momentum $\left\langle\vec{l}\right\rangle$. Hence, if the vectors $\left\langle\vec{l}\right\rangle$ and $\vec{e}$ are non-collinear the energy of the atomic electron interaction with the electromagnetic wave depends on the mutual orientation of these two vectors.

Notice, if it is assumed that atom during the whole process of light-atom interaction is unpolarized, i.e. $a_{nlm} = a_{nl}$, then the effective energy reads as

$$\langle nl|\, M\,|nl\rangle = \frac{1}{2l+1}\sum_{m=-l}^{l}\langle nlm|\, M\,|nlm\rangle.$$

In this case the diagonal compound matrix element $\langle np|\, M\,|np\rangle$ is

$$\begin{gathered}\langle np|\, M\,|np\rangle = \tfrac{1}{3}\sum_{m=-1}^{1}\langle npm|\, M\,|npm\rangle = \\ = \sum_{n'}\Big[E_{n's}\,\langle np\,\|j_1(z)\|\,n's\rangle^2 + E_{n'p}\Big(\langle np\,\|j_0(z)\|\,n'p\rangle^2 + 2\,\langle np\,\|j_2(z)\|\,n'p\rangle^2\Big) + \\ +\,E_{n'd}\Big(2\,\langle np\,\|j_1(z)\|\,n'd\rangle^2 + 3\,\langle np\,\|j_3(z)\|\,n'd\rangle^2\Big)\Big].\end{gathered} \tag{39}$$

One can see that the effective energy of $|np\rangle$ states averaged over the angular momentum projections does not depend on the polarization vector orientation. It should be noted that the

approximation $a_{nlm} = a_{nl}$ can have some sense only in the case when atom interacts with the unpolarized light.

So, one can see that there is a cardinal difference between the diagonal elements of equations (26) and (34). The compound matrix elements M_{nn} approach E_n only in the limit of the very weak fields. It is evident that the non-diagonal matrix elements of these two sets of equations differ most principally. The non-diagonal compound matrix elements for transitions $|ns\rangle \rightarrow |n's\rangle$ are

$$\begin{gathered}\langle ns|\, M\,|n's\rangle = \sum_{n''}\left[E_{n''s}\,\langle ns\,\|j_0(z)\|\,n''s\rangle\,\langle n''s\,\|j_0(z)\|\,n's\rangle + \right.\\ \left. +3E_{n''p}\,\langle ns\,\|j_1(z)\|\,n''p\rangle\,\langle n''p\,\|j_1(z)\|\,n's\rangle + 5E_{n''d}\,\langle ns\,\|j_2(z)\|\,n''d\rangle\,\langle n''d\,\|j_2(z)\|\,n's\rangle\right].\end{gathered} \tag{40}$$

For transitions $|ns\rangle \rightarrow |n'pm\rangle$ they are

$$\begin{gathered}\langle ns|\, M\,|n'pm\rangle|_{m=0} = \\ = i\sqrt{3}\cos\theta\sum_{n''}\left[E_{n''s}\,\langle ns\,\|j_0(z)\|\,n''s\rangle\,\langle n''s\,\|j_1(z)\|\,n'p\rangle + \right.\\ +E_{n''p}\,\langle ns\,\|j_1(z)\|\,n''p\rangle\,(\langle n''p\,\|j_0(z)\|\,n'p\rangle + 2\,\langle n''p\,\|j_2(z)\|\,n'p\rangle)\\ \left. +E_{n''d}\,\langle ns\,\|j_2(z)\|\,n''d\rangle\,(2\,\langle n''d\,\|j_1(z)\|\,n'p\rangle + 3\,\langle n''d\,\|j_3(z)\|\,n'p\rangle)\right],\end{gathered} \tag{41}$$

$$\begin{gathered}\langle ns|\, M\,|n'pm\rangle|_{m=\pm1} = \\ = \mp i\sqrt{\tfrac{3}{2}}\sin\theta e^{\pm i\phi}\sum_{n''}\left[E_{n''s}\,\langle ns\,\|j_0(z)\|\,n''s\rangle\,\langle n''s\,\|j_1(z)\|\,n'p\rangle + \right.\\ +E_{n''p}\,\langle ns\,\|j_1(z)\|\,n''p\rangle\,(\langle n''p\,\|j_0(z)\|\,n'p\rangle + 2\,\langle n''p\,\|j_2(z)\|\,n'p\rangle) + \\ \left. +E_{n''d}\,\langle ns\,\|j_2(z)\|\,n''d\rangle\,(2\,\langle n''d\,\|j_1(z)\|\,n'p\rangle + 3\,\langle n''d\,\|j_3(z)\|\,n'p\rangle)\right].\end{gathered} \tag{42}$$

It is seen that in contrast to the dipole selection rules the states $|ns\rangle$ and $|n'pm = \pm1\rangle$ are coupled if the vectors $\left\langle \vec{l} \right\rangle$ and $\vec{e}$ are non-collinear.

Additionally, the states of the same parity are also coupled. For example, for transitions $|ns\rangle \rightarrow |n'dm\rangle$ we have

$$\begin{gathered}\langle ns|\, M\,|n'dm\rangle|_{m=0} = \\ = -\tfrac{1}{28\sqrt{5}}\,(1+3\cos2\theta)\sum_{n''}\left[35E_{n''s}\,\langle ns\,\|j_0(z)\|\,n''s\rangle\,\langle n''s\,\|j_2(z)\|\,n'd\rangle + \right.\\ +E_{n''p}\,\langle ns\,\|j_1(z)\|\,n''p\rangle\,(42\,\langle n''p\,\|j_1(z)\|\,n'd\rangle + 63\,\langle n''p\,\|j_3(z)\|\,n'd\rangle)\\ \left. +E_{n''d}\,\langle ns\,\|j_2(z)\|\,n''d\rangle\,(35\,\langle n''d\,\|j_0(z)\|\,n'd\rangle + 50\,\langle n''d\,\|j_2(z)\|\,n'd\rangle + 90\,\langle n''d\,\|j_4(z)\|\,n'd\rangle)\right],\end{gathered} \tag{43}$$

$$\begin{gathered}\langle ns|\, M\,|n'dm\rangle|_{m=\pm1} = \\ = \pm\tfrac{1}{14}\sqrt{\tfrac{3}{10}}\sin2\theta e^{\pm i\phi}\sum_{n''}\left[35E_{n''s}\,\langle ns\,\|j_0(z)\|\,n''s\rangle\,\langle n''s\,\|j_2(z)\|\,n'd\rangle + \right.\\ +E_{n''p}\,\langle ns\,\|j_1(z)\|\,n''p\rangle\,(42\,\langle n''p\,\|j_1(z)\|\,n'd\rangle + 63\,\langle n''p\,\|j_3(z)\|\,n'd\rangle) + \\ \left. +E_{n''d}\,\langle ns\,\|j_2(z)\|\,n''d\rangle\,(35\,\langle n''d\,\|j_0(z)\|\,n'd\rangle + 50\,\langle n''d\,\|j_2(z)\|\,n'd\rangle + 90\,\langle n''d\,\|j_4(z)\|\,n'd\rangle)\right],\end{gathered} \tag{44}$$

$$\begin{gathered}\langle ns|\, M\,|n'dm\rangle|_{m=\pm2} = \\ = -\tfrac{1}{14}\sqrt{\tfrac{3}{10}}\sin^2\theta e^{\pm i2\phi}\sum_{n''}\left[35E_{n''s}\,\langle ns\,\|j_0(z)\|\,n''s\rangle\,\langle n''s\,\|j_2(z)\|\,n'd\rangle + \right.\\ +E_{n''p}\,\langle ns\,\|j_1(z)\|\,n''p\rangle\,(42\,\langle n''p\,\|j_1(z)\|\,n'd\rangle + 63\,\langle n''p\,\|j_3(z)\|\,n'd\rangle) + \\ \left. +E_{n''d}\,\langle ns\,\|j_2(z)\|\,n''d\rangle\,(35\,\langle n''d\,\|j_0(z)\|\,n'd\rangle + 50\,\langle n''d\,\|j_2(z)\|\,n'd\rangle + 90\,\langle n''d\,\|j_4(z)\|\,n'd\rangle)\right].\end{gathered} \tag{45}$$

Thus, the selection rules which determine the limits of summation on the right-hand-side of equations (26) and (34) are drastically different for these two sets of equations.

In conclusion of this subsection, let us notice some additional remarkable properties of matrix elements V_{nm}, which will be very important for future analysis. Firstly, the polarization vector $\vec{e}(t)$ has been defined as follows: $\vec{A}(t) = \vec{e}(t) A(t)$. In the case of linearly polarized wave we have $\vec{e}(t) = \vec{e}_0$ and field amplitude $A(t)$ varies in time. However, in the case of circularly polarized wave we have the opposite situations: $A(t) = A_0$ and $\vec{e}(t) = \vec{n}_x \cos(\omega t) + \vec{n}_y \sin(\omega t)$. Taking this into account it is absolutely clear that the width of nonlinear atomic response spectrum in the case of linearly polarized wave exceeds significantly that for circularly polarized wave. Indeed, the reduced matrix elements are the nonlinear functions of $A(t)$. Hence, in the case of linearly polarized wave the matrix elements $\langle n_2 l_2 \| j_l(z) \| n_1 l_1 \rangle$ will include a lot of harmonics of laser pulse carrier frequency. Contrary, in the case of circularly polarized wave the reduced matrix elements do not depend on time and the nonlinear response can be only associated with the angular part of matrix elements V_{nm}. Secondly, the normalization and orthogonality properties (12) result in the following equation

$$S_n = \sum_{m=0}^{\infty} |V_{nm}|^2 = 1,$$

where summation over m is made over the whole spectrum of atomic states. The spectrum of any atom includes the infinite number of discrete spectrum states and the uncountable number of continuum spectrum states. Hence, to solve the set of equations for probability amplitudes we should restrict ourselves by some finite number of the most important states. Let us introduce the following sum

$$S_n^{(N)} = \sum_{m=0}^{N} |V_{nm}|^2. \tag{46}$$

The numerical value of this sum depends on field amplitude and it does not exactly equal unity in whole range of the field strength variation. At the same time the sum $S_n^{(N)}$ can serve as a measure of completeness of the finite basis of eigenfunctions. Fig. 2 shows the sum (46) as a function of field strength for the case of hydrogen atom. One can see that the basis of the eigenfunctions consisting of 6 low-lying discrete and 280 continuum states can be considered as complete basis in the following range of laser field strength: $0 < \mu_0 \leqslant 1$. It should be noted, that the further increase in the number of states will not result in sufficient increase of calculation accuracy.

3. Atom response field

3.1 Polarization features of the response field

In the far-field range the spectrum of vector potential of atomic response field is given by

$$\vec{A}_r(\vec{r}, \omega) = \frac{\exp(ikr)}{rc} \int \vec{j}(\vec{r}', \omega) \exp\left(-i\vec{k}\vec{r}'\right) dV',$$

where $\vec{j}(\vec{r}, \omega)$ is the spectrum of atomic current density, which is defined by the well known expression (Landau, 1981)

$$\vec{j}(\vec{r}, t) = \frac{q}{2m} \left[\psi^* \cdot \left(\vec{p} - \frac{q}{c}\vec{A}\right) \psi + \left(\left(\vec{p} - \frac{q}{c}\vec{A}\right) \psi\right)^* \cdot \psi\right]. \tag{47}$$

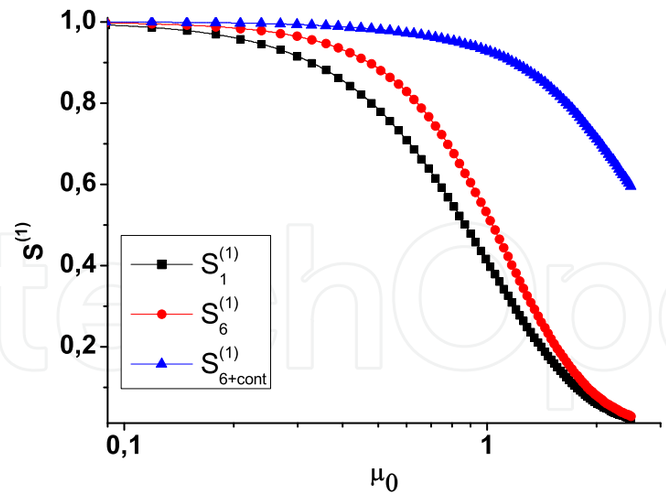

Fig. 2. The sum $S_n^{(N)}$ as a function of parameter μ_0 for the different finite sets of hydrogen atom eigenfunctions

In its turn the spectral density of response field intensity is given by

$$\frac{dI}{d\omega} = \frac{c}{4}\left|B_r\left(\vec{r},\omega\right)^2\right| r^2 do = \frac{\omega^2}{4c^3}\left|\int\left[\vec{j}\left(\vec{r}',\omega\right)\vec{n}\right]\exp\left(-i\vec{k}\vec{r}'\right)dV'\right|^2 do. \tag{48}$$

In the case when the long-wave approximation, $ka_0 << 1$ (where a_0 is the amplitude of electron oscillation in external field), holds for any harmonic, the intensity spectrum of single atom response is given by

$$\frac{dI}{d\omega} = \frac{\omega^2}{4c^3}\left|\left[\vec{J}\left(\omega\right)\vec{n}\right]\right|^2 do, \tag{49}$$

where

$$\vec{J}\left(\omega\right) = \int \vec{j}\left(\vec{r},\omega\right)dV. \tag{50}$$

However, if we deal with the spatially distributed ensemble of atoms, the equation (50) takes the form

$$\vec{J}\left(\vec{k},\omega\right) = \sum_{i=1}^{N}\vec{J}_i\left(\omega\right)\exp\left[i\left(\vec{k}\vec{r}_i - \omega t_i\right)\right], \tag{51}$$

where $\vec{r}_i$ is the coordinate of i-th atom of ensemble. Let $\vec{k}_0$ is the wave vector of the incident electromagnetic wave. Then the phase of the field in the position of i-th atom is $\omega_0 t - \vec{k}_0\vec{r}_i = \omega_0\left(t - t_i\right)$, where $t_i = \vec{k}_0\vec{r}_i/\omega_0$. By substituting t_i into the equation (51) we get

$$\vec{J}\left(\vec{k},\omega\right) = \sum_{i=1}^{N}\vec{J}_i\left(\omega\right)\exp\left[i\frac{\omega}{c}\left(\vec{n}\left(\omega\right) - \vec{n}_0\left(\omega_0\right)\right)\vec{r}_i\right],$$

where $\vec{n}\left(\omega\right) = \vec{k}c/\omega$ and $\vec{n}_0\left(\omega_0\right) = \vec{k}_0 c/\omega_0$. If the atoms of ensemble are identical it is convenient to introduce the form factor $f\left(\vec{k},\vec{k}_0\right)$ which is defined by

$$\vec{J}\left(\vec{k},\omega\right) = \vec{J}\left(\omega\right)\sum_{i=1}^{N}\exp\left[i\frac{\omega}{c}\left(\vec{n}\left(\omega\right) - \vec{n}_0\left(\omega_0\right)\right)\vec{r}_i\right] = \vec{J}\left(\omega\right)f\left(\vec{k},\vec{k}_0\right). \tag{52}$$

It is seen that the form factor takes into account the retardation effects, which depend on the dispersive properties of atomic media and the geometry of the radiative volume. Let us illustrate the difference between the frequency-angular spectra of single atom and spatially distributed ensemble of atoms. In the case of Gaussian incident beam the density of responding atoms in illuminating area can be approximated as follows

$$\frac{N}{V}(\vec{r}) = \frac{N_0}{V}\frac{\theta(z + L/2 - \theta z - L/2)}{2}\exp\left(-\frac{\rho^2}{\rho_0^2}\right),$$

where $\theta(z)$ is the unit step function, ρ_0 is the beam radius, and L is the length of gas volume in direction of the laser pulse propagation. We assume that the z axis is directed along the direction of the wave vector $\vec{k}_0$ of the incident wave, and the wave vector of the response field is defined by $\vec{k} = \{k\sin\theta\cos\varphi, k\sin\theta\sin\varphi, k\cos\theta\}$. In this case the form factor $f(\theta,\omega)$ defined by Eq. (52) takes the following form

$$f(\theta,\omega) = \frac{\sin\left[kL\left(n(\omega)\cos\theta - n_0(\omega_0)\right)/2\right]}{kL\left(n(\omega)\cos\theta - n_0(\omega_0)\right)/2}\exp\left[-\frac{1}{4}\left(k\rho_0 n(\omega)\sin\theta\right)^2\right],$$

It is seen from the last equation that if we neglect the atomic media dispersive properties, i.e. if we assume $|\vec{n}(\omega)| = |\vec{n}_0(\omega_0)| = 1$, then the intensity of all harmonics reaches the maximum at $\theta = 0$. However, if we take into account the dispersive properties of the atomic ensemble then we get the conical emission. The intensity of different harmonics reaches maximum at different angles θ_N with respect to the direction of the laser pulse wave vector. It is well known that the refraction index $n(\omega)$ is varied significantly in the visible and UV ranges and approaches unity in XUV spectral range. So, it is supposed that the frequency-angular spectrum of emission is strongly varied in the visible and UV ranges and becomes more rigid in XUV and x-ray region.

The matrix elements of the generalized momentum operator $\vec{P} = \vec{p} - q\vec{A}/c$ in sets of eigenfunctions for problems (7) and (9) appear as

$$\int u_n^*(\vec{r})\left(\vec{p} - \frac{q}{c}\vec{A}\right)u_m(\vec{r})\,dV = \sum_{k,p} V_{nk}^{-1}(t)\,\vec{p}_{kp}V_{pm}(t), \tag{53}$$

$$\int \varphi_n^*(\vec{r},t)\left(\vec{p} - \tfrac{q}{c}\vec{A}\right)\varphi_m(\vec{r},t)\,dV = \int u_n^*(\vec{r})\,\vec{p}\,u_m(\vec{r})\,dV = \vec{p}_{nm},$$

respectively. Substituting (25) into (47) with the use of (53) for the total current of atomic electrons, we obtain

$$\vec{J}(t) = \frac{q}{m}\sum_{n,m,p,q} a_n^*(t)\,a_m(t)\,V_{np}^{-1}(t)\,\vec{p}_{pq}V_{qm}(t). \tag{54}$$

Note that Eq. (53) manifests the relation between the matrix elements of generalized momentum and the matrix elements of momentum in the basis of free atom eigenfunctions $\vec{p}_{nm} = -i\hbar\int u_n^*(\vec{r})\,\vec{\nabla}u_m(\vec{r})\,dV$. In contrast to the generalized momentum matrix elements, the matrix elements of momentum operator $\vec{p}$ are directly related with the coordinate matrix elements $\vec{p}_{nm} = im\omega_{nm}\vec{r}_{nm}$. So, finally, we get

$$\vec{J}(t) = i\sum_{n,m,p,q} a_n^*(t)\,a_m(t)\,\omega_{pq}V_{np}^{-1}(t)\,\vec{d}_{pq}V_{qm}(t). \tag{55}$$

We should recall that the probability amplitudes $a_n(t)$ are the coefficients of wavefunction expansion into series of free atom eigenfunctions, so all summation indexes are three-dimensional values $n = (n, l, m)$. Using these 3D representation for the partial matrix elements of expression (55), we get

$$\langle n_1 l_1 m_1 | \vec{J} | n_2 l_2 m_2 \rangle = i \sum_{n_3 l_3 m_3} \sum_{n_4 l_4 m_4} \left(\omega_{n_3 l_3} - \omega_{n_4 l_4} \right) \langle n_1 l_1 m_1 | V^{-1} | n_3 l_3 m_3 \rangle \langle n_3 l_3 m_3 | \vec{d} | n_4 l_4 m_4 \rangle \langle n_4 l_4 m_4 | V | n_2 l_2 m_2 \rangle , \tag{56}$$

where $\omega_{nl} = E_{nl}/\hbar$ and E_{nl} are the energy eigenvalues for the free atom problem. Using the angular momentum summation rules, for the dipole operator $\vec{d}$ we obtain

$$\langle n_3 l_3 m_3 | \vec{d} | n_4 l_4 m_4 \rangle = q \langle n_3 l_3 \| r \| n_4 l_4 \rangle (-1)^{m_3} i^{l_4 - l_3} \sqrt{(2l_3 + 1)(2l_4 + 1)} \cdot \cdot \sum_{m=-1}^{1} \vec{n}^{(m)} \begin{pmatrix} l_3 & 1 & l_4 \\ -m_3 & m & m_4 \end{pmatrix} \begin{pmatrix} l_3 & 1 & l_4 \\ 0 & 0 & 0 \end{pmatrix},$$

here

$$\vec{n}^{(0)} = -i\vec{n}_z, \quad \vec{n}^{(\pm)} = \pm i \frac{\vec{n}_x \mp i\vec{n}_y}{\sqrt{2}}$$

The matrix elements of the operator V have been calculated above. So, Eq. (56) can be transformed as

$$\langle n_1 l_1 m_1 | \vec{J} | n_2 l_2 m_2 \rangle = 4\pi q i^{l_2 - l_1 + 1} \sqrt{(2l_1 + 1)(2l_2 + 1)} \sum_{n_3 l_3} \sum_{n_4 l_4} \left(\omega_{n_3 l_3} - \omega_{n_4 l_4} \right) (2l_3 + 1)(2l_4 + 1) \cdot \cdot \sum_{l=|l_1 - l_3|}^{l_1 + l_3} \sum_{l'=|l_2 - l_4|}^{l_2 + l_4} \sqrt{(2l + 1)(2l' + 1)} \langle n_1 l_1 \| j_l \| n_3 l_3 \rangle \langle n_3 l_3 \| r \| n_4 l_4 \rangle \langle n_4 l_4 \| j_{l'} \| n_2 l_2 \rangle \cdot \cdot \begin{pmatrix} l_1 & l & l_3 \\ 0 & 0 & 0 \end{pmatrix} \begin{pmatrix} l_3 & 1 & l_4 \\ 0 & 0 & 0 \end{pmatrix} \begin{pmatrix} l_4 & l' & l_2 \\ 0 & 0 & 0 \end{pmatrix} \cdot \sum_{m=-1}^{+1} \sum_{m_3=-l_3}^{l_3} (-1)^{l' - m_2 + m_3} Y_{l(m_3 - m_1)}(\vec{e}) \vec{n}^{(m)} Y_{l'(m_3 - m_2 - m)}(\vec{e}) \cdot \cdot \begin{pmatrix} l_1 & l & l_3 \\ -m_1 & m_1 - m_3 & m_3 \end{pmatrix} \begin{pmatrix} l_3 & 1 & l_4 \\ -m_3 & m & m_3 - m \end{pmatrix} \begin{pmatrix} l_4 & l' & l_2 \\ m_3 - m & m_2 - m_3 + m & -m_2 \end{pmatrix}, \tag{57}$$

where, as previously, $j_l = j_l(qA(t)\, r/\hbar c)$.

Thus, the mathematical formalism of this section allows us to calculate the angular-frequency spectrum (AFS) of the atomic response field in the case of arbitrary mutual orientation of the angular momentum of the atom and the external field polarization if it is linearly polarized, as well as for arbitrary state of its polarization. As follows from (57), the polarization of AFS components depends on both angular momentum direction and polarization vector of the incident field.

3.2 Atom response at subatomic laser field strength

We now comprehend the main characteristics of the response field in the subatomic range at $\mu << 1$. Matrix elements of dipole momentum are nonzero for the states with angular momentums shifted to unity: $l' = l \pm 1$. As mentioned above, the diagonal reduced matrix elements $\langle n_1 l_1 \| j_0 \| n_1 l_1 \rangle$ are the even functions of the field amplitude and at $\mu << 1$ take values close to unity. Reduced matrix elements $\langle n_1 l_1 \| j_1 \| n_3 (l_1 \pm 1) \rangle$ are the odd functions and at $\mu \to 0$ vary as the first power of the field $\langle n_1 l_1 \| j_1 \| n_3 (l_1 \pm 1) \rangle \sim \mu$. All other matrix elements have noticeably smaller values because they vary as higher powers of the field $\langle n_1 l_1 \| j_1 \| n_3 l_1 \rangle \sim \mu^2$ when $n_3 \neq n_1$, and $\langle n_1 l_1 \| j_1 \| n_3 (l_1 \pm k) \rangle \sim \mu^k$.

We now proceed with the analysis of diagonal matrix elements of the atomic current. Taking into account the above considerations for the most valuable contributions in the subatomic range, we obtain

$$\begin{gathered}\left\langle n_1 l_1 m_1\right|\vec{J}\left|n_1 l_1 m_1\right\rangle = \sum_n k\left(n_1 l_1, nl\right)\left\langle n_1 l_1 \left\| j_0 \right\| n_1 l_1\right\rangle\left\langle n_1 l_1 \left\| r \right\| nl\right\rangle\left\langle nl \left\| j_1 \right\| n_1 l_1\right\rangle \cdot \\ \sum_{m=-1}^{+1} \vec{n}^{(m)} Y_{1m}\left(\vec{e}\right) \sum_{m'=-1}^{+1}\left\langle l_1 m_1\right| Y_{1m}\left(\vec{n}\right)\left|l m'\right\rangle\left\langle l m'\right| Y_{1m}^{*}\left(\vec{n}\right)\left|l_1 m_1\right\rangle,\end{gathered} \tag{58}$$

where $l = l_1 \pm 1$. For brevity, we have introduced the new term $k\left(n_1 l_1, nl\right)$, the explicit expression of which can be found from comparison of (58) and (57). Performing summation over m', for the angular dependence of the matrix elements (58), we obtain

$$\vec{F}_{l_1 m_1}\left(\vec{n}, \vec{e}\right) = \sum_{m=-1}^{+1} \vec{n}^{(m)} Y_{1m}\left(\vec{e}\right) C_m\left(l_1 m_1\right), \tag{59}$$

where

$$\left\{\begin{array}{c} C_1\left(l_1 m_1\right) \\ C_0\left(l_1 m_1\right) \\ C_{-1}\left(l_1 m_1\right) \end{array}\right\} = \frac{1}{\left(2l_1+1\right)\left(2l_1+2\right)\left(2l_1+3\right)} \cdot \left\{\begin{array}{c} \left(l_1 - m_1 + 1\right)\left(l_1 - m_1 + 2\right) \\ 2\left(l_1 + m_1 + 1\right)\left(l_1 - m_1 + 1\right) \\ \left(l_1 + m_1 + 1\right)\left(l_1 + m_1 + 2\right) \end{array}\right\}. \tag{60}$$

Specifically,

$$C_m\left(l_1 = 0\right) = \frac{1}{3}, \quad \sum_{m_1=-l_1}^{l_1} C_m\left(l_1 m_1\right) = \frac{1}{3}.$$

Thus, from equations (59), (60) it follows that the direction of atomic current coincides with the external field polarization vector only in the case of atom with zero angular momentum $l_1 = 0$, or non-polarized ensemble of atoms, i.e. when the sublevels of atomic energy structure are degenerated: $a_{n_1 l_1 m_1}\left(t\right) = a_{n_1 l_1}\left(t\right)$. Indeed, in these cases, we obtain

$$\sqrt{12\pi}\sum_{m_1} \vec{F}_{l_1 m_1}\left(\vec{n}, \vec{e}\right) = \sqrt{\frac{4\pi}{3}} \sum_{m=-1}^{+1} \vec{n}^{(m)} Y_{1m}\left(\vec{e}\right) = \vec{e}. \tag{61}$$

At the same time, Eq. (58) shows that in general case the direction of atomic current diagonal matrix elements depend on both external field and angular momentum directions. In principle, because the eigenvalues of both "free atom" and "atom in the field" boundary value problems depend on the two quantum numbers (nl) only, the matrix elements $\left\langle n_1 l_1 m_1\right|\vec{J}\left|n_1 l_1 m_1'\right\rangle$ could be treated as diagonal. However, in the external field, the shifts appear between the sublevels of different m. Hence, the latter approximation can be valid only in the case when these shifts are negligible. Thus, in general case the atomic current diagonal matrix elements posses the tensor structure and depend on both external field and angular momentum directions.

Now, we turn to analysis of the nondiagonal matrix elements of atomic current. Taking into account the properties of reduced matrix elements $\left\langle n' l' \left\| j_l \right\| n'' l''\right\rangle$ at subatomic field strength, we find that the main contribution comes from the term

$$\begin{gathered}\left\langle n_1 l_1 m_1\right|\vec{J}\left|n_2 l_2 m_2\right\rangle = k\left(n_1 l_1, n_2 l_2\right)\left\langle n_1 l_1 \left\| j_0 \right\| n_1 l_1\right\rangle\left\langle n_1 l_1 \left\| r \right\| n_2 l_2\right\rangle \cdot \\ \cdot\left\langle n_2 l_2 \left\| j_0 \right\| n_2 l_2\right\rangle \sum_{m=-1}^{+1} \vec{n}^{(m)}\left\langle l_1 m_1\right| Y_{1m}\left(\vec{n}\right)\left|l_2 m_2\right\rangle,\end{gathered} \tag{62}$$

where $l_2 = l_1 \pm 1$, and coefficient $k(n_1 l_1, n_2 l_2)$ has been introduced above. It is seen that in contrast to diagonal matrix elements, these depend exclusively on the angular momentum direction and not on the external field direction:

$$\vec{F}_{l_1 m_1, l_2 m_2}(\vec{n}) = \sum_{m=-1}^{+1} \vec{n}^{(m)} \langle l_1 m_1 | Y_{1m}(\vec{n}) | (l_1 \pm 1) m_2 \rangle. \tag{63}$$

In subatomic fields, as follows from (27), matrix element $\langle nl \| j_0 \| nl \rangle \approx 1$; therefore,

$$\langle n_1 l_1 m_1 | \vec{J} | n_2 l_2 m_2 \rangle = k(n_1 l_1, n_2 l_2) \langle n_1 l_1 m_1 | \vec{r} | n_2 l_2 m_2 \rangle. \tag{64}$$

Hence, the selection rules for nondiagonal current matrix elements $l_1 \to l_2 = l_1 \pm 1$ agree with the dipole selection rules governed by the angular momentum of the atom, and the directions of matrix elements $\langle n_1 l_1 m_1 | \vec{J} | n_2 l_2 m_2 \rangle$ in nonpolarized media are completely chaotic.
The population amplitudes in the subatomic range are calculated using perturbation theory if there are no resonances between the pulse carrier frequency and the frequencies of atomic transitions. Under the assumption that $|a_{N_0}(t)| \approx 1$, Eqs. (26) yield

$$\begin{gathered} a_{N_0}(t) = a_{N_0} \exp[-i\Phi_0(t)], \\ a_{N_1}(t) = a_{N_0} \exp[-i\Phi_1(t)] \cdot \int_{-\infty}^{t} M_{N_1 N_0}(t') \exp[i(\Phi_1(t') - \Phi_0(t'))] dt', \end{gathered} \tag{65}$$

where $\Phi_i(t) = \frac{1}{\hbar} \int_{-\infty}^{t} M_{N_i N_i}(t') dt'$. As mentioned above, in the subatomic range, the matrix elements between neighboring states $l_0 \to l_1 = l_0 \pm 1$ make the maximal contribution. For such transitions, Eq. (35) takes the form

$$\begin{gathered} M_{N_1 N_0}(t) = \sqrt{12\pi} i^{l_0 - l_1} (-1)^{m_0} \sqrt{(2l_1 + 1)(2l_0 + 1)} \langle n_1 l_1 \| j_1 \| n_0 l_0 \rangle \\ \left(E_{n_1 l_1} \langle n_1 l_1 \| j_0 \| n_1 l_1 \rangle + E_{n_0 l_0} \langle n_0 l_0 \| j_0 \| n_0 l_0 \rangle \right) \begin{pmatrix} l_1 & 1 & l_0 \\ -m_1 & m_1 - m_0 & m_0 \end{pmatrix} \begin{pmatrix} l_1 & 1 & l_0 \\ 0 & 0 & 0 \end{pmatrix} Y_{1(m_0 - m_1)}(\vec{e}). \end{gathered} \tag{66}$$

In particular, for diagonal matrix elements, we obtain

$$M_{N_1 N_1}(t) = E_{n_1 l_1} (\langle n_1 l_1 \| j_0 \| n_1 l_1 \rangle)^2. \tag{67}$$

So, for the nondiagonal term of the total atomic current, we finally obtain

$$\begin{gathered} \vec{J}_{N_1 N_0}(t) = a^*_{N_1}(t) a_{N_0}(t) \langle n_1 l_1 m_1 | \vec{J} | n_0 l_0 m_0 \rangle = |a_{N_0}|^2 k_1(n_1 l_1, n_0 l_0) \langle n_1 l_1 \| j_0(t) \| n_1 l_1 \rangle \\ \langle n_1 l_1 \| r \| n_0 l_0 \rangle \langle n_0 l_0 \| j_0(t) \| n_0 l_0 \rangle \exp[i(\varphi_1(t) - \varphi_0(t))] \\ \int_{-\infty}^{t} dt' \langle n_1 l_1 \| j_1(t') \| n_0 l_0 \rangle \left(E_{n_1 l_1} \langle n_1 l_1 \| j_0(t') \| n_1 l_1 \rangle + E_{n_0 l_0} \langle n_0 l_0 \| j_0(t') \| n_0 l_0 \rangle \right) \cdot \\ \cdot \exp[-i(\varphi_1(t') - \varphi_0(t'))] \sum_{m=-1}^{+1} \vec{n}^{(m)} Y_{1m}(\vec{e}(t')) C_m(l_1 m_1, l_0 m_0), \end{gathered} \tag{68}$$

where

$$C_m(l_1 m_1, l_0 m_0) = \begin{pmatrix} l_1 & 1 & l_0 \\ -m_1 & m & m_0 \end{pmatrix}^2.$$

For example, in the case when $l_1 = l_0 + 1$, for the coefficients $C_m\left(l_1 m_1, l_0 m_0\right)$ with the use of relation $m_1 = m_0 + m$, we obtain

$$\left\{ \begin{array}{c} C_1\left(l_0 m_0\right) \\ C_0\left(l_0 m_0\right) \\ C_{-1}\left(l_0 m_0\right) \end{array} \right\} = \frac{1}{(2l_0+1)(2l_0+2)(2l_0+3)} \cdot \left\{ \begin{array}{c} \left(l_0 + m_0 + 1\right)\left(l_0 + m_0 + 2\right) \\ 2\left(l_0 - m_0 + 1\right)\left(l_0 + m_0 + 1\right) \\ \left(l_0 - m_0 + 1\right)\left(l_0 - m_0 + 2\right) \end{array} \right\}.$$

3.3 Atomic response in the case of impact of two linearly polarized pulses

We now examine the situation when an atom interacts with the superposition of two linearly polarized pulses with arbitrary directions of polarization vectors $\vec{e}_1$ and $\vec{e}_2$:

$$\vec{A}\left(t\right) = \vec{e}_1 A_1\left(t\right) + \vec{e}_2 A_2\left(t\right), \tag{69}$$

where $A_{1,2}\left(t\right)$ are the magnitudes of vector potentials of laser field components, which can be represented as an envelope with harmonic stuffing:

$$A_{1,2}\left(t\right) = f_{1,2}\left(t\right)\cos\left(\omega_{1,2} t + \varphi_{1,2}\right),$$

here $\omega_{1,2}$ are the carrier frequencies, $f_{1,2}\left(t\right)$ are the pulse envelopes, and $\varphi_{1,2}$ are the phase shifts. Apparently, the spatial direction of the superposed field changes during the pulse propagation:

$$\vec{A}\left(t\right) = \vec{e}_1 A_1\left(t\right) + \vec{e}_2 A_2\left(t\right) = \vec{e}\left(t\right) A\left(t\right).$$

To clarify our interpretation, we turn to a certain special case without loss of generality. We assume that vector $\vec{e}_1$ is directed along the z axis in the laboratory system of coordinates and vector $\vec{e}_2$ lies in the (y, z) plane and makes an angle θ_0 with the z axis. Then, the vectors $\vec{A}_{1,2}\left(t\right)$ look like

$$\vec{A}_1\left(t\right) = \left\{0, 0, A_1\left(t\right)\right\}, \quad \vec{A}_2\left(t\right) = \left\{0, A_2\left(t\right)\sin\theta_0, A_2\left(t\right)\cos\theta_0\right\}.$$

Therefore, vector $\vec{A}\left(t\right)$ should always lie in the (y, z) plane and make an angle $\theta\left(t\right)$ with the z axis, which is found to be

$$\theta\left(t\right) = \arctan\frac{A_2\left(t\right)\sin\theta_0}{A_1\left(t\right) + A_2\left(t\right)\cos\theta_0}. \tag{70}$$

In addition, the vector $\vec{e}\left(t\right)$ and magnitude of vector $\vec{A}\left(t\right)$ are determined as follows

$$\vec{e}\left(t\right) = \left\{0, \sin\theta\left(t\right), \cos\theta\left(t\right)\right\}, \tag{71}$$

$$A\left(t\right) = A_1\left(t\right)\cos\theta\left(t\right) + A_2\left(t\right)\cos\left(\theta_0 - \theta\left(t\right)\right). \tag{72}$$

It is seen that angle $\theta\left(t\right)$ does not vary in time exclusively under the circumstances of equality of amplitudes $A_1\left(t\right) = A_2\left(t\right)$ or collinear geometry $\theta_0 = \pi n$.

Hence, the problem of polychromatic field interaction with an ensemble of atoms requires special examination even in the simplest case, when the ensemble consists of a single atom, because the direction of the total polarization vector is generally time-dependent. Equation (70) shows that in noncollinear geometry, this effect remains even in the case of identical carrier frequencies ($\omega_1 = \omega_2$) and pulse envelopes, but with some delay between them ($A_2\left(t\right) = A_1\left(t - t_0\right)$). In the linear regime, the response to a superposition of fields appears to be a superposition of responses to each component, but the nonlinear interaction makes the whole picture rather more complicated.

4. Numerical research

The application of the developed method to the study of atomic response specific features in laser fields of near-atomic strength is presented below.
In computer simulations we shall assume that the laser pulse has the Gaussian temporal profile

$$\vec{A} = \vec{e}A_0 \exp\left(-\frac{(t-t_0)^2}{\tau_0^2}\right)\sin(\omega t), \tag{73}$$

where ω is the laser pulse carrier frequency and τ_0 is the pulse temporal width. The delay time t_0 does not play any significant role and we have chosen it to place pulse peak at the center of integration interval.

4.1 Selection rules

In Section 2 we have already discussed the principle differences between the set of equations for probability amplitudes, which follow from the Hamiltonian in electro-dipole approximation (34), and equations (26) of the proposed theory. Indeed, the angular momentum selection rules of equations (26) are not restricted by condition $\Delta l = \pm 1$ of the electro - dipole approximation theory. For example, this difference will manifest itself in the angular distribution of photoelectron emission.
Let us consider the process of hydrogen atom ionization by electromagnetic wave with the carrier frequency of $\hbar\omega = 15.11eV$. Because the quantum energy exceeds the binding energy of $1s$ electron, then in this case we have the one-quantum ionization. As a result the energy-level diagram can be approximated by the following way. We take into account the ground state and continuum spectrum states with the angular momentum values lying in the interval $l = 0 - 5$. The energy interval of continuum spectrum states which should be taken into account is determined by the energy dependency of reduced matrix elements (19). This dependency is non monotonic and reach maximum at certain value of ionized electron wave number, $E_{max} = \hbar^2 {k_{max}}^2/2m$. The matrix element $\langle 1s|V|k_{max}l\rangle$ as a function of field strength for transitions from the ground state to the continuum spectrum states of different angular momentum $l = 0 - 5$ are shown in Fig. 3. It is seen that the dimensionless parameter μ_0 is varied in the interval $\mu_0 = (0.01 - 5)$, it corresponds to the variation of the laser pulse intensity in the interval $I = 2.16 \cdot 10^{12} - 5.4 \cdot 10^{17}$ W/cm^2.
It is seen, that in the region of subatomic field strength the magnitude of matrix elements $\langle 0|V|k_{max}, l = 1\rangle$ exceeds the magnitude of all other elements (this region is marked as "I" in Fig.3). Such ratio of matrix elements of different multipolarity transitions indicates that in this region of laser field amplitude the selection rules, associated with the traditional electro-dipole allowed transitions, play the dominant role. However, when the field amplitude approach the near-atomic field strength the magnitude of matrix elements for $\Delta l = 2$ transition becomes initially equal and then exceeds the magnitude of $\Delta l = 1$ transition (the region II). Further increase of the laser field amplitude results in the successive increase of magnitude of matrix elements for transitions $\Delta l = 3$, $\Delta l = 4$, etc. Hence, the electro-dipole selection rules are violated in the region of over-atomic field strength. In the region II the most probable transition become the transition corresponding to the selection rule of $\Delta l = 2$. In the region III there is no any preferred transition.
As we have mentioned above, the profiles of angular spectra of photoelectron emission corresponding to different Δl transitions are different. The results of computer simulations have shown that in the region of subatomic field strength the angular distributions are

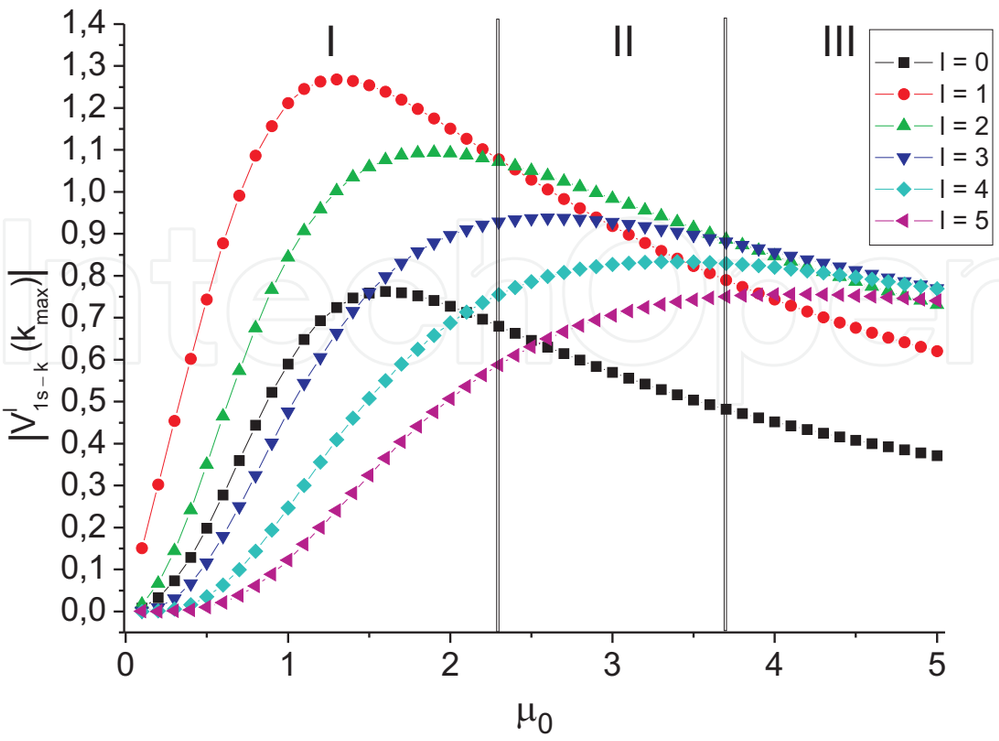

Fig. 3. Maximum value of matrix elements as a function of parameter μ_0. Angular momentum l runs from 0 to 5.

described by the Legendre function of the first order. Such distributions correspond to the electro-dipole transitions. With the increase of the pulse intensity the additional lobes in angular distribution of low energy photoelectrons appear. The angular distribution of the high energy photoelectrons remains approximately invariable. Fig. 4 shows the angular distributions of photoelectron emission for the case of laser pulse of field strength $\mu_0 = 5$ ($I = 5.4 \cdot 10^{17}$ W/cm^2). The angular distributions are averaged in time over the laser pulse duration. It is seen that the multilobe directional pattern for low energy photoelectrons is transformed to the unidirectional angular distribution for high energy photoelectrons. In the case of intense ultrashort laser pulses the angular spectra demonstrate the specific feature consisting in the asymmetry of emission in direction along (0°) and opposite (180°) to polarization vector. We suppose that this asymmetry is due to the fact that $A(t)$ given by (73) is odd function of time. From the general point of view, it is evident that the most energetic photoelectrons arise in time interval near the maximum of the instantaneous laser field strength. For the laser pulse of time profile (73) the maximum of the field strength magnitude corresponds to its negative value. This is in agreement with the curve (c) in the Fig. 4. It is also evident that the width of the energy region, where the selection rules differ from the electro-dipole one, grows with the increase of laser pulse intensity.

4.2 Ionization probability as a function of laser field amplitude

As we have mentioned in Introduction the first consistent theory of atom ionization has been proposed by Keldysh (Keldysh, 1965). Keldysh's theory is based on the model atom having only one bound state. If it is assumed that the wave functions of continuum spectrum states can be calculated in quasiclassical approximation then the probability of ionization reads as

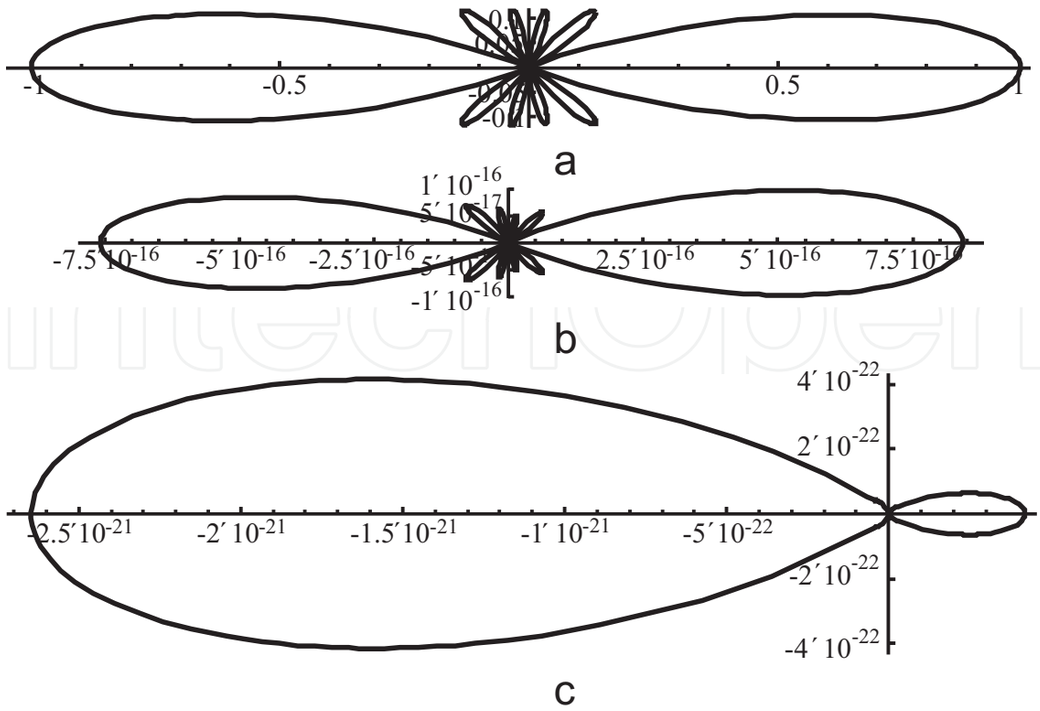

Fig. 4. Angular distributions of photoelectrons with $(a)\, k = 0.05$, $(b)\, k = 0.95$, $(c)\, k = 4.55$ at the external field amplitude $\mu_0 = 5$

$$w_{Keld}(\mu_0) \sim \exp\left[-2Im\left[\int_{\tau}^{\tau_0} \mu_0^2 \sin^2(\frac{\hbar\omega}{E_i}\tau')d\tau' + \tau_0\right]\right], \tag{74}$$

where E_i is the binding energy of electron, and ω is the carrier frequency of electromagnetic field. According to Eq. (74) the probability of ionization increases monotonically with the field strength in subatomic region, and it is saturated in the region of the over-atomic field strength. Here, we shall demonstrate that if we take into account the multi-level structure of the discrete spectrum states then the ionization probability ceases to be a monotonic function of field strength. The integral probability of ionization is defined as the total population of the continuum spectrum states after the termination of the laser pulse action

$$w_{ion} = \sum_{k,l,m} |a_{k,lm}\,(t \to \infty)\,|^2. \tag{75}$$

To specify the process under consideration let us turn on to the silver atom interaction with the pulses of *Ti:Sapphire* laser at wavelength 800 *nm*. The spectrum of the discrete and continuum states of silver is infinite, as for any other atom in nature. Neither analytical nor numerical research allows us to take into account all of them. Therefore, we need for a mathematical criterion for the selection of states making a substantial contribution to the process of light–atom interaction. This becomes extremely important because we have gone beyond the approximations of perturbation theory and, hence, the resonant transitions cease to play any significant role in the dynamics of level populations. As we have mentioned in Sec.2 the role of such criterion play the sum $S_n^{(N)}$.

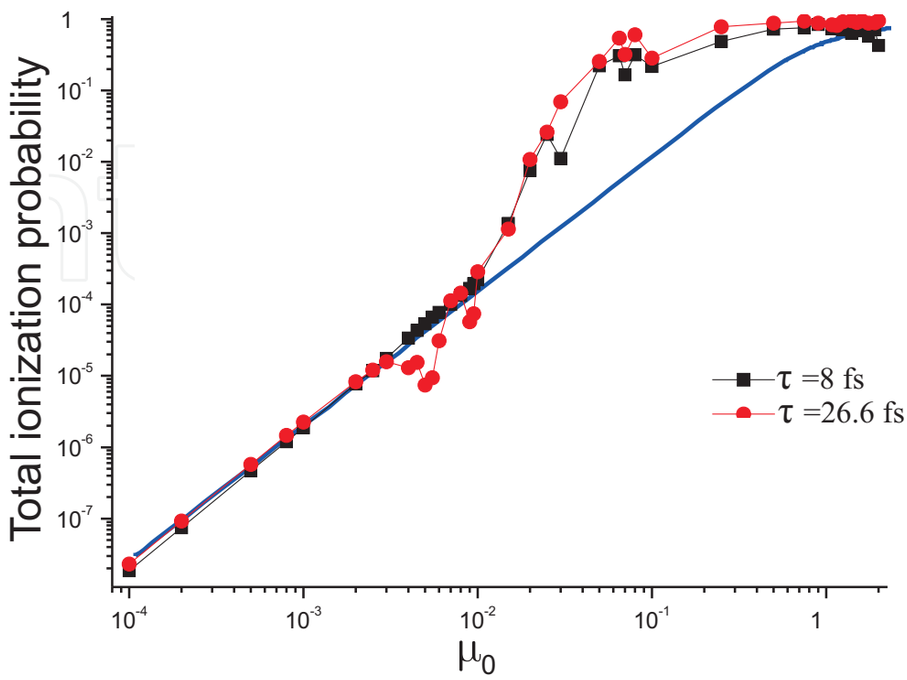

Fig. 5. Total ionization probability as a function of laser field amplitude μ_0 ($\lambda = 800$nm)

Fig. 5 shows the total ionization probability as a function of laser field strength for the case of atomic silver ionization by $Ti : Sapphire$ laser pulses of duration: $\tau = 3T$ (squares) and $10T$ (circles). Solid line depicts ionization probability dependence calculated on the base of Keldysh model (Keldysh, 1965), in frame of which it is supposed that atom has only one bound state. From this figure we see, that in the region of substantially subatomic fields ($\mu_0 \leq 10^{-3}$) ionization rate actually does not depend on pulse duration and coincide with the curve, predicted by Keldysh model. At the same time in near-atomic field $10^{-3} \leq \mu_0 \leq 4 \cdot 10^{-1}$ this dependence demonstrate some new features: it ceases to be monotonic function; it depends not only on field strength, but also on pulse duration, i.e. on pulse energy. One more peculiarity is that ionization probability gets not only larger magnitudes than the Keldysh curve has, but also smaller. In the region $\mu_0 \geq 4 \cdot 10^{-1}$ ionization probability saturates.

4.2.1 Subatomic fields

Fig. 6 shows the population of discrete and continuum spectrum states after the termination of laser pulse as a function of field strength for the two values of the $Ti : Sapphire$ laser pulse temporal width: $\tau = 10T$ (a,b) and $3T$ (c,d). As it is seen from fig. 5, for the case of pulse duration of $\tau = 3T$ the ionization probability is well-fitted by Keldysh curve till the values $\varphi \leq 10^{-2}$. In this region, as fig.6 c shows, the population of excited states rises monotonically with the laser field strength. The total population of all excited states is less than tenth part of percent and the population of $5p$ level exceeds populations of higher levels. For the case of $\tau = 10T$ the region of agreement with Keldysh formula extends to $\mu_0 \leq 2.5 \cdot 10^{-3}$. In this case we also observe monotonic growth of discrete state populations. The distribution

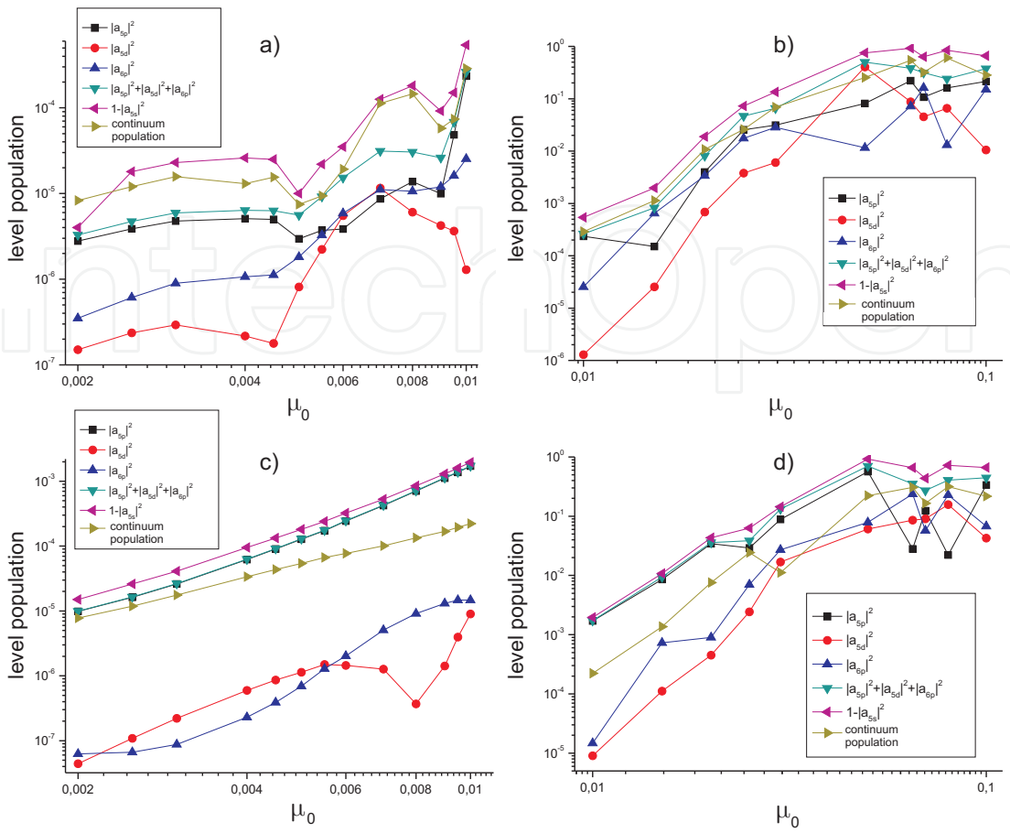

Fig. 6. Post-pulse population of silver atom energy states as a function of laser field strength for pulse temporal width $\tau = 10T$ (a,b) and $3T$ (c,d) ($\lambda = 800$nm)

of population of discrete spectrum states is "quasiequilibrium", i.e. the population of upper states exceeds lower ones. At the same time, the total population of excited states is still less than hundredth of percent.

Summarizing, we can say, that a good agreement with Keldysh model is observed when the ionization from ground state is dominating process, while the population of excited states is small and increases monotonically with the laser field strength.

4.2.2 Ionization stabilization

At pulse duration $\tau = 10T$ and field strength $\mu_0 \geq 2.5 \cdot 10^{-3}$ the ionization probability gets the values less, than predicted by Keldysh model. Such decrease in ionization probability is usually called by ionization stabilization effect (see, e.g. (Popov, 2004)). Fig. 6 a provides a clear explanation of this effect. Indeed, one can see, that in this region the population of all discrete states is saturated. This is conditioned by the fact that the rate of population is determined not only by the transitions from ground state, but also by recombination transitions. As it is seen from fig.6 a, at $\mu_0 \geq 2.5 \cdot 10^{-3}$ the rates of these processes first equalize, and then at $\mu_0 \approx 5 \cdot 10^{-3}$ the rate of recombination processes starts to prevail. This dominating effect expresses in the fact that at $\varphi \geq 5 \cdot 10^{-3}$ the populations of excited states are equalized, and the ground state population decreases, which means that the population distribution more and more decline from "quasiequilibrium" one. Addressing to fig. 1a, one

can see, that the reason of this declination consists in nonlinearity of the M_{nm} dependence on field strength. Notice another specific feature of the process. By comparing figs. 6a and 6c we can see that the level populations depend not only on field strength, but also on pulse duration i.e. on pulse energy. We can also see that the temporal dynamics of population distribution in multilevel atom results not only in the ionization stabilization but also in suppression of ionization rate with external laser field growth.
Note, that figures represented above demonstrate that the model of atom with one or even a few discrete states is insufficient for the consistent interpretation of yielded data, because the distribution of level populations changes non-monotonically. This non-monotonic character of the dynamics is conditioned by the competition between three kind of the processes: ionization, recombination, and interlevel transitions within the discrete band. The final populations depend essentially on ratio between the rates of these three processes.

4.2.3 Enhanced ionization

At field strength $\mu_0 \geq 10^{-2}$ the ionization probability starts to exceed values, predicted by Keldysh curve. This phenomenon has quite obvious explanation associated with the temporal dynamics of population of discrete spectrum states. Figs. 6b and 6d represent post-pulse population dependence as a function of field strength. It is seen that total population of excited discrete states exceeds 10% at field strength $\mu_0 = 3 \cdot 10^{-2}$, which means that contribution from this states becomes noticeable. In spite of the fact that in the case $\tau = 10T$ the integral population of the continuum spectrum states is close to the integral population of discrete spectrum states, the energy density of continuum state population, $d|a|^2/dE$, is small, because the energy width of photoionization cross section (see, fig.1b) increases rapidly in the region of near-atomic field strength. As a result, in this region of field strength the processes of ionization starting from the excited bound states become to play the dominating role. In spite of the fact that the rate of ionization exceeds the value predicted by Keldysh's model this enhancement can be explained in the frame of the Keldysh theory. Indeed, the parameter γ of Keldysh's theory depends on the ratio $N_0 = U_0/\hbar\omega$, which determines how much photons need to overcome the ionization threshold U_0. It is evident that N_0 decreases with the decrease of binding energy U_0. Hence, the ionization from the excited states became dominant.

4.2.4 Ionization rate saturation

In fig. 5 one can see, that at $\mu_0 > 0.1$ the ionization probability starts to saturate and that is to be associated with its approaching to unity. Such kind of the dependence is predictable from general point of view and the fact that our numerical results agree with this evident circumstance and nowhere exceeds unity verify the fact that our theory is non-perturbative (Andreev, 2009; 1999; 2006; 2007; 2008; 2010), i.e. it is not restricted by the small values of ratio E/E_{at}. Furthermore, in full agreement with properties of matrix elements showed in fig. 1a, the atomic silver ionization probability under action of laser pulse of duration $\tau = 3T$ starts to fall at field strength $E > E_{at}$.

4.3 Photoemission spectrum of atomic response

We now analyze the photoemission spectra of atomic silver response. The photoemission spectra for some values of the laser field strength are shown in Fig 7. In the region of substantially subatomic field strength ($\mu_0 < 10^{-4}$) the spectrum of response include only the fundamental frequency of incident pulse. Hence, in this case the response is linear. The odd harmonics appear in spectrum with the field strengthening and their amplitudes rapidly

fall with the harmonic number. At the field strength $\mu_0 \sim 10^{-3}$ we see quantitative changes in the spectrum profile: its width grows and the plateau with pronounced cut-off frequency arises. Further field strengthening leads to the strengthening of these tendencies: spectrum width considerably grows and cut-off frequency gets more contrast ($\mu_0 = 1.2 \cdot 10^{-2}$).

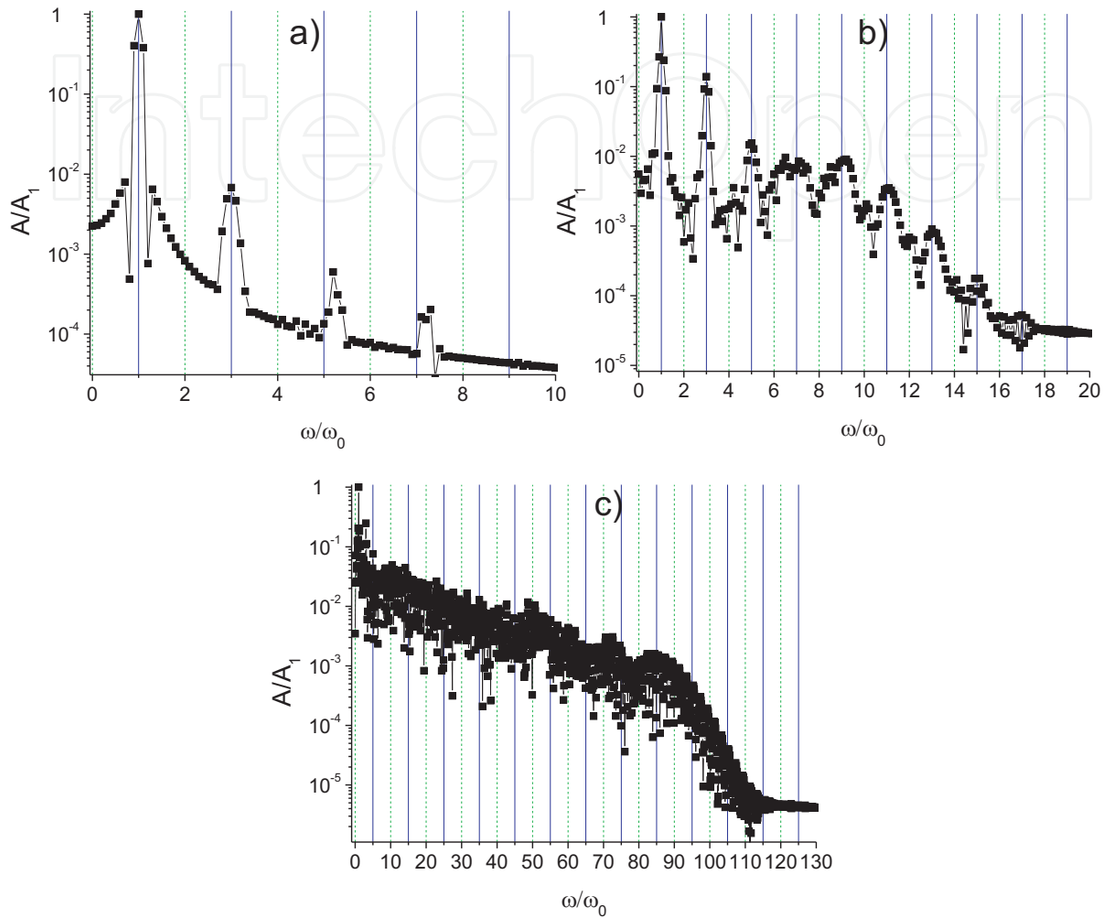

Fig. 7. The photoemission spectra generated in silver at $\mu_0 = 0.0045$ (a), $\mu_0 = 0.025$ (b), $\mu_0 = 0.08$ (c)

The dependence of cut-off frequency on the laser field strength is shown in fig. 8. One can see that in the weak field range ($\mu_0 < 0.1$) there is the quadratic growth of cut-off frequency with the field strength. However, at laser pulse intensity $I > 10^{14}\, W/cm^2$ the CF is saturated, i.e. it ceases to be intensity dependent. The reason of such behavior is quite obvious if we take into account that the probability of electron ionization approaches unity in this region of pulse intensity (see fig. 5). It means that the atomic electron is mostly localized in the continuum spectrum states and it does not collide with its parent ion. At the same time, as far as the time profile (73) of laser pulse has relatively soft slope in front of pulse, hence, the harmonics are effectively generated here. So, the results of computer modeling show that the most probable reason of the cutoff frequency saturation is the total ionization of the irradiated atom.

Some interpretation of such modification of response spectra can be done with the help of analytic solutions (65) obtained in perturbation theory approximation. To avoid the overcomplicated mathematical expressions for definition of CF let us concentrate on the

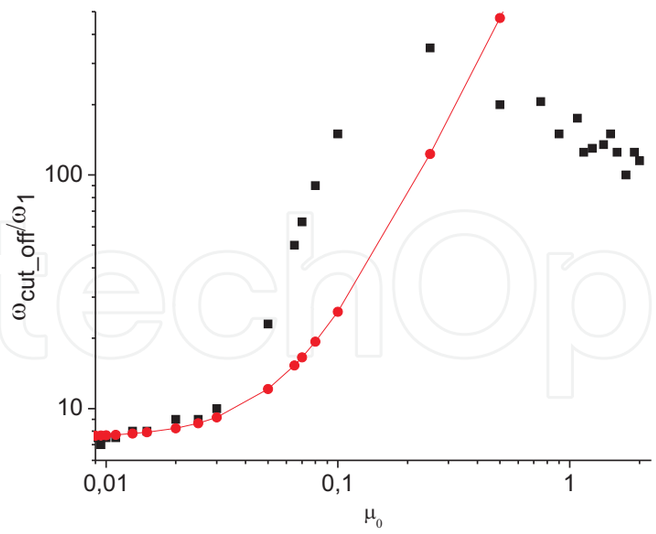

Fig. 8. Cut-off frequency as a function of laser pulse intensity. The solid red curve is the approximated quadratic dependence

hydrogen atom. In subatomic region of the laser field strength we can restrict ourselves by account of the two lowest discrete states and quadratic approximation for the compound matrix elements

$$M_{2p}(t) \approx E_{2p}\left(1 - 10\mu^2(t)\right), \quad M_{1s}(t) \approx E_{1s}\left(1 - \mu^2(t)\right). \tag{76}$$

Here we have signed $M_n = M_{nn}$ for brevity. Assuming that incident pulse profile has the form (73) and executing time integration, we find the expression for $\Phi_n(t)$

$$\Phi_{2p}(t) - \omega_{2p}t = \\ = -\omega_{2p}\sqrt{\frac{\pi}{2}}\frac{5\mu_0^2\tau_0}{4}\left[2\mathrm{erf}\left(\frac{\sqrt{2}t}{\tau_0}\right) + i\exp\left(-\frac{\omega_0^2\tau_0^2}{2}\right)\left(\mathrm{erfi}\left(\frac{-2it+\omega_0\tau_0^2}{\tau_0}\right) - \mathrm{erfi}\left(\frac{2it+\omega_0\tau_0^2}{\tau_0}\right)\right)\right] \tag{77}$$

$$\Phi_{1s}(t) - \omega_{1s}t = \\ = -\omega_{1s}\sqrt{\frac{\pi}{2}}\frac{\mu_0^2\tau_0}{8}\left[2\mathrm{erf}\left(\frac{\sqrt{2}t}{\tau_0}\right) + i\exp\left(-\frac{\omega_0^2\tau_0^2}{2}\right)\left(\mathrm{erfi}\left(\frac{-2it+\omega_0\tau_0^2}{\tau_0}\right) - \mathrm{erfi}\left(\frac{2it+\omega_0\tau_0^2}{\tau_0}\right)\right)\right], \tag{78}$$

where $\mathrm{erf}(z)$ is the error function and $\mathrm{erfi}(z) = \mathrm{erf}(iz)/i$. The first term in square brackets describes energy shift governed by pulse profile and the second one shows oscillations with double carrier frequency. The second term equals zero, when external pulse has rectangular profile, and is negligibly small, when external pulse has Gaussian profile and its duration satisfies the condition $\omega_0\tau_0 >> 1$. Then in subatomic region ($\mu_0 << 1$) the phases $\Phi_i(t)$ are finally approximated by the following expressions

$$\Phi_{2p}(t) = \omega_{2p}\left[t - \frac{5}{2}\sqrt{\frac{\pi}{2}}\mu_0^2\tau_0\tanh\left(\frac{\sqrt{3}t}{\tau_0}\right)\right],$$

$$\Phi_{1s}(t) = \omega_{1s}\left[t - \frac{1}{4}\sqrt{\frac{\pi}{2}}\mu_0^2\tau_0\tanh\left(\frac{\sqrt{3}t}{\tau_0}\right)\right].$$

Therefore, during the laser pulse action the level energy spacing depends on time and the instantaneous frequency reads as

$$\Omega(t) = \frac{d}{dt}\left(\Phi_{2p}(t) - \Phi_{1s}(t)\right) = \omega_{2p} - \omega_{1s} - \sqrt{\frac{3\pi}{2}}\mu_0^2\left(\frac{5}{2}\omega_{2p} - \frac{1}{4}\omega_{1s}\right)\cosh^{-2}\left(\frac{\sqrt{3}t}{\tau_0}\right).$$

It is seen, that the magnitude of energy shift is

$$\Delta\omega = \sqrt{\frac{3\pi}{2}}\mu_0^2\left(\frac{5}{2}\omega_{2p} - \frac{1}{4}\omega_{1s}\right). \tag{79}$$

Energy shift $\Delta E = \hbar|\Delta\omega|$ in hydrogen-like atom for transition $1s \to 2p$ is found then to be

$$\Delta E = \sqrt{\frac{3\pi}{2}}\frac{3}{4}U_p,$$

where U_p is ponderomotive potential, given by well-known expression

$$U_p = \frac{e^2E_0^2}{4m\omega^2}.$$

In the previous section we have discussed the difference between the diagonal ($n = m$) and non-diagonal ($n \neq m$) partial matrix elements of atomic current. As we have seen, the diagonal elements result in sequence of odd harmonics. At the same time, the shape of spectra resulted from the non-diagonal elements depends significantly on the laser pulse spectral width. In the case of a few–cycle laser pulses this part of the integral spectrum takes the shape of quasi-continuum plateau, spread till double energy shift of Eq. (6), instead of a sequence of distinct harmonics. Hence, in the subatomic region of field strength the cutoff energy, E_c, can be estimated as

$$E_c = \frac{3}{2}\sqrt{\frac{3\pi}{2}}U_p = 3.26 \cdot U_p.$$

It is seen that the obtained equation coincides approximately with the well known semi-empirical equation $E_c = U_0 + 3.17 \cdot U_p$.

Let us remind that Eq. (79) is true only in subatomic region at $\mu_0 \ll 1$, when the approximation (76) for compound matrix elements is legal. In Sec.2.4 we have shown that the reduced matrix elements fall with field strength in the region $\mu_0 \geq 1$. It is this property of matrix elements that provides the mathematical explanation of cut-off frequency saturation in over-atomic fields.

The similar calculations can be easily made for the case of silver atom. However, the appropriate equations have the very cumbersome form, therefore we shall not bring them here. The approximated analytical dependence calculated for silver atom is shown in Fig. 8 by solid line with circles. In the region of the laser pulse intensity of $\left(10^{11} \leq I \leq 10^{12}\right)\ W/cm^2$ the results of computer calculations are in good agreement with the approximate equation. This agreement is due to the following. The dependency described by solid line has been derived under account of only two discrete states, namely $5s$ and $5p$. On the other hand, in this region of pulse intensity the population of $5p$ state exceeds significantly the population of other excited states of discrete spectrum, as it has been shown in previous section. Under further increase in the laser pulse intensity the quadratic curve raises faster than the numerically calculated curve. In this region of pulse intensity the population of other discrete spectrum excited states becomes comparable and, due to the recombination process, even exceeds the population of $5p$ state. Hence, the above approximation ceases to be valid.

4.4 Atom interaction with two-color laser field

Let us now turn to the problem of atom interaction with two-color laser field. As a practical example of the problem we shall consider the THz emission in argon gas, because there is number of available data of experimental measurements. The incident laser field constitutes of the fundamental frequency and second harmonic of *Ti* : *Sapphire* laser. The main goal of research is to study the modification of photoemission spectrum under variation of laser field parameters (field amplitudes, pulse durations, delay times, and angles between polarization vectors of components). We have mentioned in Introduction that the traditional interpretation of experiments on THz emission in two-color laser fields follows the theoretical description of THz emission in monochromatic laser field, which is usually based on the four-wave-mixing rectification (FWMR) process in laser produced plasma. Here, we are going to show that in multi-color fields the atomic nonlinearities take the dominant role and may prevail over the plasma nonlinearities. Therefore, in the computer simulations we shall assume that the laser pulse intensity is below the ionization threshold intensity. In accordance with this assumption we shall take into account the thirteen low-lying states of argon atom. The degree of completeness of the chosen set of eigenfunctions is determined by the sum $S_n^{(N)}$ (see Eq. (46)). So, our calculations show that in the region of the laser field strength $\mu_0 < 0.1$ the chosen set of eigenstates is practically complete. Note, that the energy difference between highest and lowest state of the modeled atom amounts to 96.5% of ionization energy of a real argon atom. The condition $\mu_0 < 0.1$ means that the laser pulse intensity is limited by the value $I < 6.77 \cdot 10^{12}$ W/cm^2).

Figure 9 shows some typical spectra of the atomic response in the case of two pulses with the following parameters: $\mu_{01} = 0.1, \mu_{02} = 0.0316, \tau_1 = 120fs, \tau_2 = 85fs$, and a delay time of 100 *fs*. Figure 9a corresponds to the collinear geometry, and Fig. 9b, to the orthogonal geometry. In the first case ($\theta = 0$), the atomic response includes even as well as odd harmonics of the external field, and in the second case ($\theta = \pi/2$), only odd harmonics. This indicates that the response symmetry features, which are strictly related to the character of the response anisotropy, are sensitive to the angle between the polarization vectors of the pulses. It should be noted that the component of the atomic response field with polarization collinear to the polarization vector of the incident field at the fundamental frequency is shown only in Fig. 9.

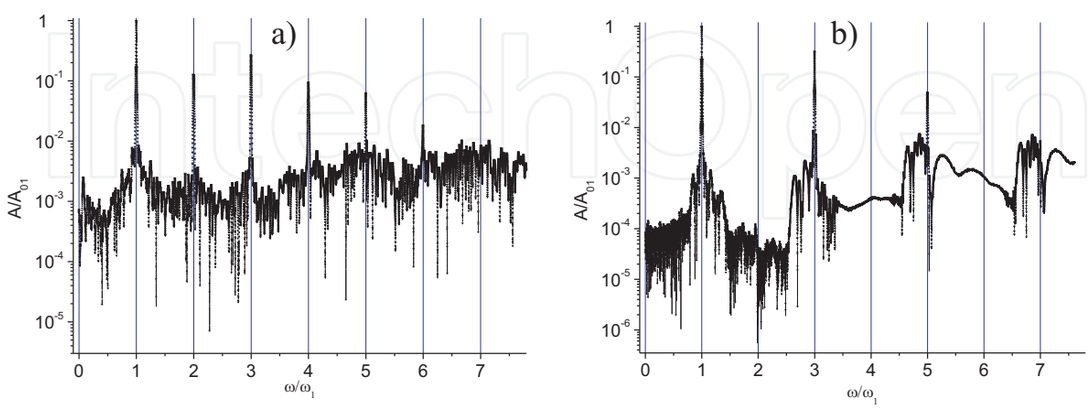

Fig. 9. Atomic response spectra: (a) collinear geometry, (b) orthogonal geometry

Figure 10 provides more detailed information on the low-frequency (THz) part of the spectra, shown in Fig 9. The enlargement of this detail of the spectrum immediately reveals that the

shape of the THz signal strongly depends on the angle between polarizations. In order to study this dependence more accurately, we varied the angle within the range $[0, \pi]$. Figure 11 represents the corresponding dependence of THz-signal output for laser pulses with parameters $\mu_{01} = 0.1, \mu_{02} = 0.1, \tau_1 = \tau_2 = 4.25fs$ and a delay of time 0 fs (a) or 13.33 fs (b). The THz-signal output is determined as the total signal recorded at a frequency of 1 THz. The most remarkable feature of this curve is its nonmonotonic behavior.

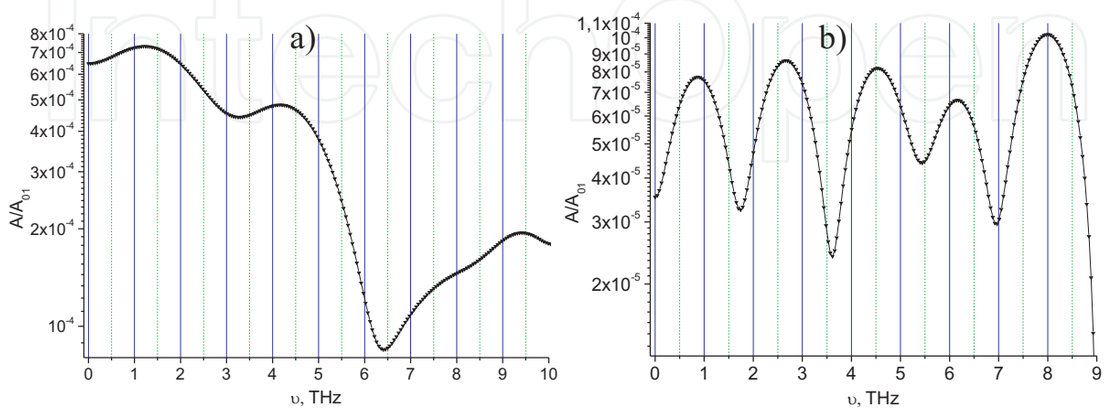

Fig. 10. THz part of atomic response spectra: (a) collinear geometry, (b) orthogonal geometry

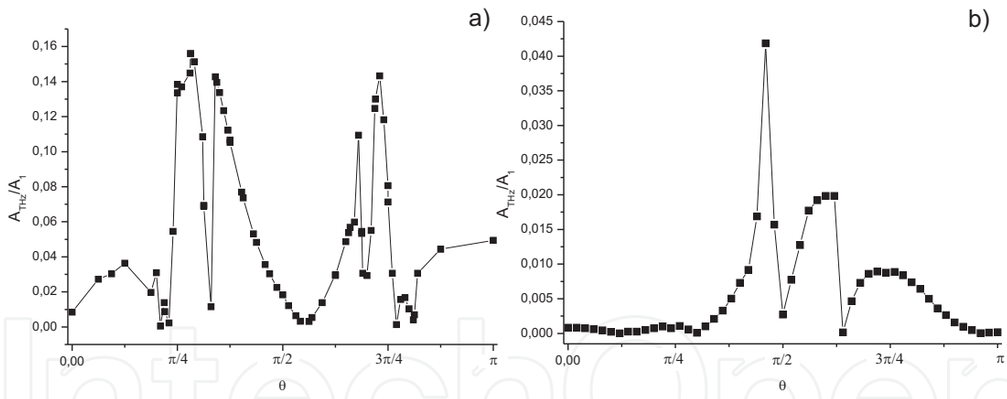

Fig. 11. THz response field amplitude as a function of angle between the polarization vectors of laser field components at frequencies ω and 2ω for $\mu_{01} = 0.1, \mu_{02} = 0.1, \tau_1 = \tau_2 = 4.25fs$ and for the delay times: 0 fs (a) 13.33 fs (b)

It is seen that a slight variation in angle may lead to a considerable change in the efficiency of THz-signal generation. Such behavior is consistent with the above discussion, and its origin is illustrated by the Fig. 12, where the trajectory described by the end of vector $\vec{A}(t)$ (see Eq.(69)) is shown. It is seen that the polarization state of the laser field depends significantly on the temporal profiles of constituents and the integral field could not be described in terms of linear, circular, or elliptic polarization.

The spectra of atomic response in the two-color laser fields depend on a number of parameters of constituent fields, which includes the amplitudes, temporal widths, delay times, and

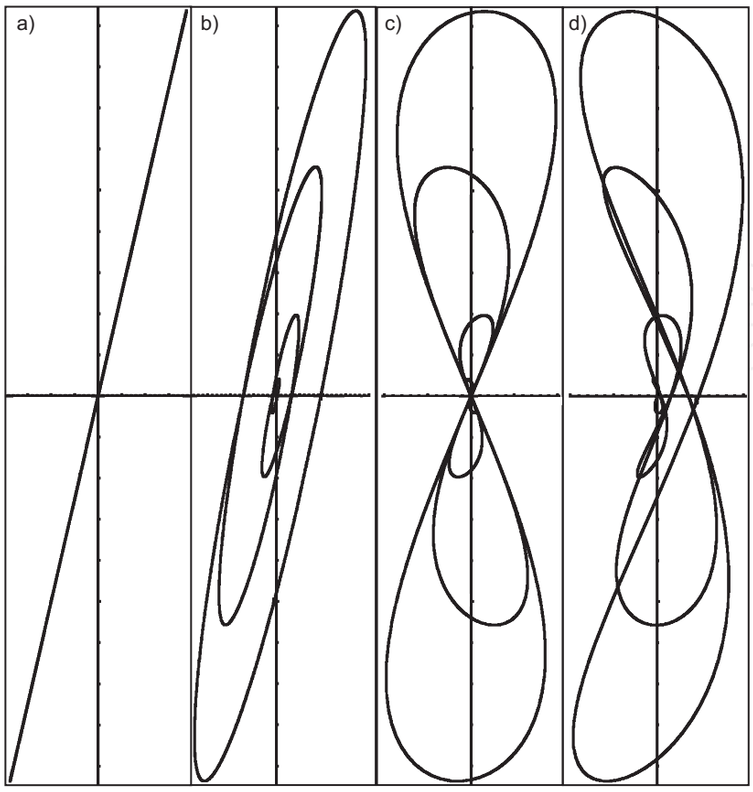

Fig. 12. Trajectory outlined by the end of integral field vector $\vec{A}(t)$ in the plane (y,z) (see (69)) for $A_{01} = 1$, $A_{02} = 0.2$, $\theta_0 = \pi/2$ and $\omega_1 = \omega_2, t_{01} = t_{02} = 0$ (a); $\omega_1 = \omega_2$, $t_{01} = 0, \omega_2 t_{02} = 0.5$ (b); $\omega_1 = 2\omega_2, t_{01} = t_{02} = 0$ (c); $\omega_1 = 2\omega_2, t_{01} = 0, \omega_2 t_{02} = 0.5$ (d)

mutual orientation of the fields at frequencies ω and 2ω. Fig. 13 illustrates the transformations of the response spectrum profile under variations of these parameters.

Figure 14 shows the angular dependence of the ninth harmonic of the fundamental frequency, which corresponds to XUV emission. By comparing Figs. 11 and 14, we can easily see the common features of the response in the long- (THz) and short- (XUV) wavelength regions. The power of emission in long and short wavelength parts of spectrum is small, if the pulses at frequencies ω and 2ω, have the same temporal profile. However, we can significantly enhance the generation efficiency by delaying the second-harmonic pulse. It should be noted again that the component of response field with the polarization collinear to polarization vector of laser field at fundamental frequency has been shown in above figures.

The dependency of the THz emission power on mutual orientation of polarization vectors of waves at frequencies ω and 2ω have been experimentally studied in recent work (Kim, 2008). The results of comparison of dependencies shown in fig.14 with the experimental data are presented in fig. 15. One can see that there is a good agreement between the results of computer simulations and in-situ measurements.

Thus, the results of computer simulations clearly demonstrate that variation in the mutual polarizations and temporal profiles of two-color field pulses is an effective tool for modifying the nonlinear atomic response spectra in a strongly controllable way.

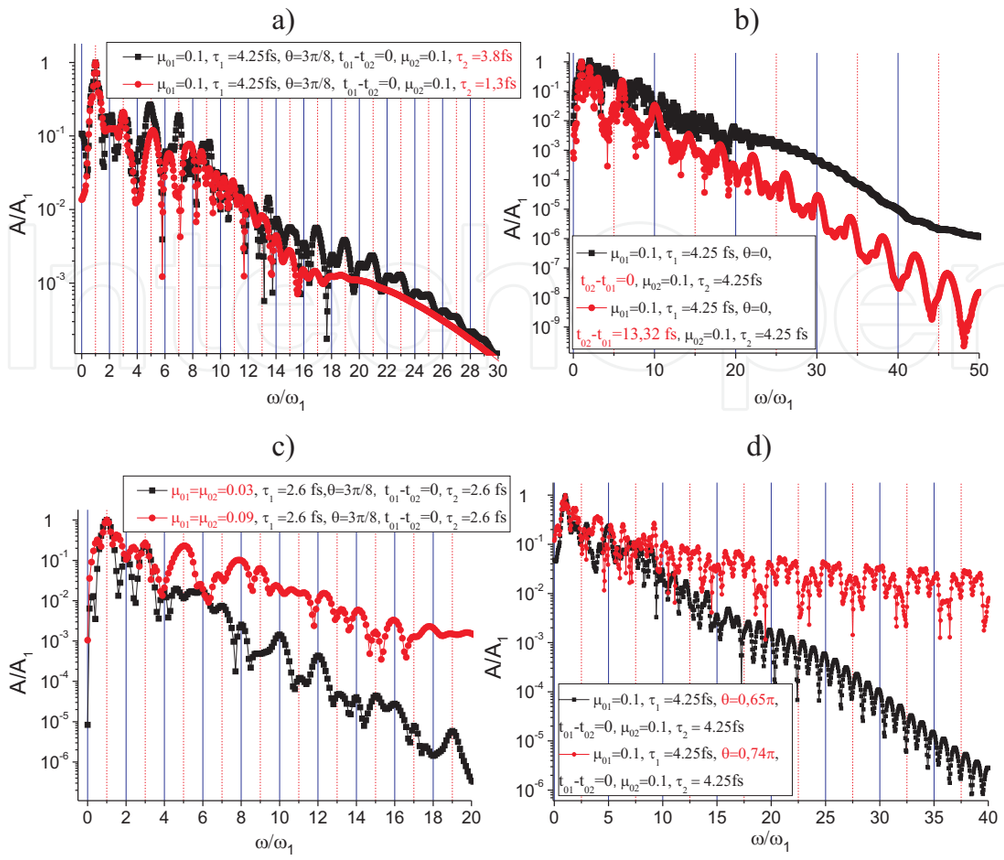

Fig. 13. Spectra of argon atom response in two-color field: (a) $\mu_{01} = \mu_{02} = 0.1, \tau_1 = 4.25fs, t_{01} - t_{02} = 0, \theta = 3\pi/8, \tau_2 = 3.8fs$ (squares) and $\tau_2 = 1.3fs$ (circles); (b) $\mu_{01} = \mu_{02} = 0.1, \tau_1 = \tau_2 = 4.25fs, , \theta = 0, t_{01} - t_{02} = 0$ (squares) and $t_{01} - t_{02} = 13.32fs$ (circles); (c) $\tau_1 = \tau_2 = 2.6fs, t_{01} - t_{02} = 0, \theta = 3\pi/8, \mu_{01} = \mu_{02} = 0.03$ (squares) and $\mu_{01} = \mu_{02} = 0.09$ (circles); (d) $\mu_{01} = \mu_{02} = 0.1, \tau_1 = \tau_2 = 4.25fs, t_{01} - t_{02} = 0, \theta = 0.65\pi$ (squares) and $\theta = 0.74\pi$ (circles)

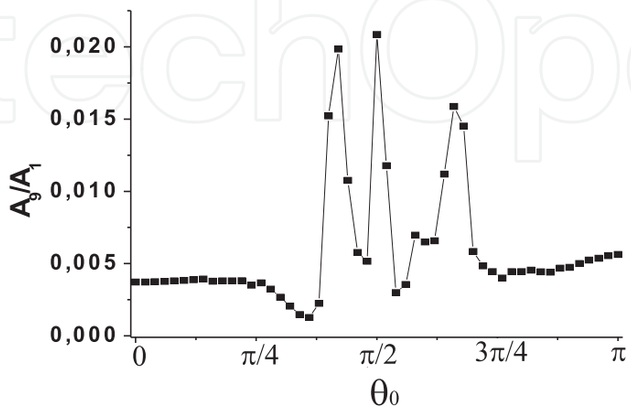

Fig. 14. Ninth harmonic field amplitude as a function of angle between the polarization vectors of laser field components at frequencies ω and 2ω

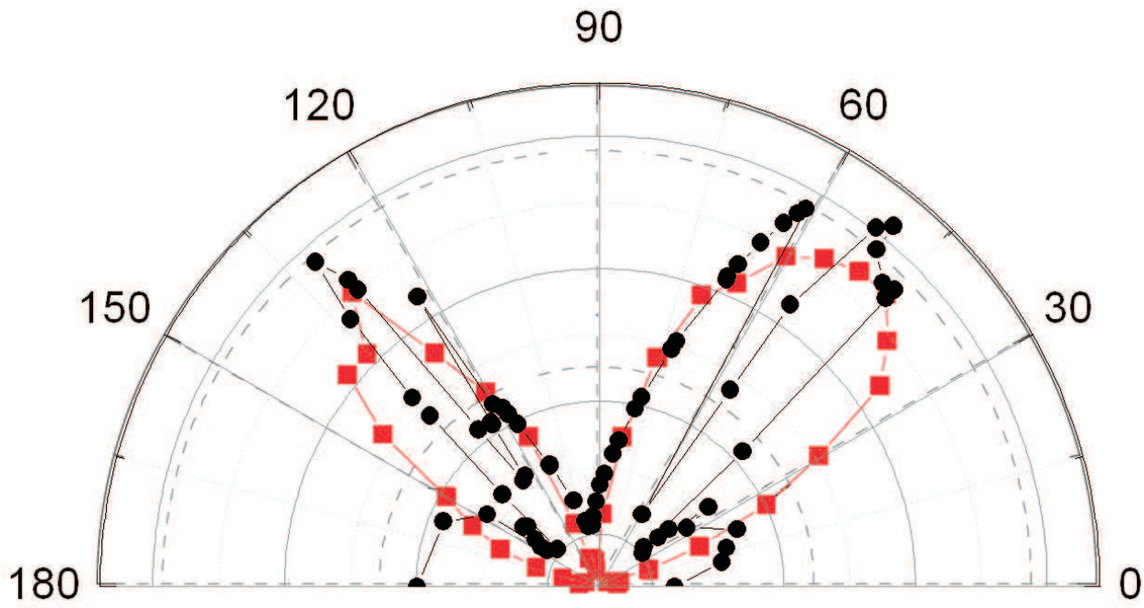

Fig. 15. THz emission power under variation of the 2ω polarization angle: experiment (squares) and computer simulations (circles)

5. Conclusions

The new theoretical approach in the theory of an atom interaction with the intense laser pulses has been developed. The proposed approach is based on the exact analytical solutions of the boundary value problem for "atom in the external field". The obtained solutions form the complete basis of the orthonormal eigenfunctions including both the discrete and continuous spectrum states. The spectrum of eigenvalues of "atom in the external field" problem coincides exactly with that for free atom boundary value problem. The eigenfunction bases of these two boundary value problems are the one-to-one sets. The transformation matrix is $\langle nlm| \exp\left(i\frac{q}{\hbar c}\vec{A}(t)\vec{r}\right)|n'l'm'\rangle$, where n is the principle quantum number, l and m are the angular momentum and its projection. For any atom with the spherically symmetric intra-atomic potential the angular part of transformation matrix is calculated in explicit analytic form; the radial part is also calculated in analytic form for the case of hydrogenic radial functions. The developed approach is non-perturbative one, because it is free of some constraints on the ratio of laser to intra-atomic field strengths. This is the most principle benefit of the developed approach. Notice, that as far as the theory is based on the Schrodinger equation we can speak here on the non-relativistic interactions. The generalization of the proposed approach for the region of relativistic field strength is given in book (Andreev, 2009). The developed theory has been applied to study the specific features of non-linear atomic response in the case of the laser pulses of near-atomic field strength and multi-color laser fields. The presented results of the mathematical modeling provide the interpretation of a number of phenomena, which has been observed experimentally and closely related to near-atomic field strength of laser pulses. (i) The violation of the electro-dipole selection rule. This phenomenon is due to the nonlinear dependency of compound matrix elements M_{nm} on the laser field strength. As it has been shown these matrix elements are linear

functions of laser field amplitude only in region of subatomic field strength. The growth of the field amplitude results in the dominating role of high order terms with respect to the degrees of field amplitude. (ii) The stabilization of ionization, enhanced ionization, and saturation of ionization rate. The nature of these phenomena is at least twofold. Firstly, the account of multilevel structure of bound atomic states affects drastically on the ionization probability dependency on the laser field strength. This is due a number of different reasons. The integral rate of level population is a sum of the rates of ionization, recombination, and interlevel transitions among the atomic discrete spectrum. Any of these rates is nonlinear function of the field amplitude. The energy width of continuum populated states is also nonlinearly depends on the field amplitude. The stabilization ionization process occurs when the recombination process becomes dominating. The enhanced ionization is due to the ionization from the excited bound states and it occurs when the population of excited discrete spectrum states becomes appreciable. The saturation of ionization probability is due to the total single ionization of an atom. (iii) The cut-off frequency saturation. The good agreement of the results of computer simulations on the silver atom photoemission spectra and experimentally measured spectra shows that the cut-off frequency saturation is due to the total single ionization. (iv) The developed theory, supported by results of computer simulations, shows that in multicolor laser fields the variation of mutual polarization of field constituents provides the most effective method of photoemission spectrum control both in short and long wavelength regions. The results of calculations of THz emission power as a function of mutual orientation of two-color field polarization vectors show that in multicolor fields the atomic response is due mainly by atomic but not plasma nonlinearities. The significant enhancement in the intensity of high harmonics under variation of mutual orientation of two-color field polarization vectors is of great practical interest as a source of intensive x-ray emission and for development of subfemtosecond pulse formation methods.

6. References

Andreev, A. V. (2009). *Relativistic Quantum Mechanics*, Fizmatlit.

Andreev, A. V. (1999). Interaction of an atom with superstrong laser fields, *Journal of Experimental and Theoretical Physics* 89(3): 421–427.

Andreev, A.V. & Shoutova, O. (2006). Single hydrogen like atom ionization by ultrastrong laser field: non-perturbative approach, *Physics Letters A* 350(3-4): 309–314.

Andreev, A.V.; Shoutova, O. . S. S. Y. (2007). Ionization of a single hydrogen-like atom by laser pulses of near-atomic strength, *Laser Physics* 17(4): 496–507.

Andreev, A.V.; Stremoukhov, S. . S. O. A. (2008). Atom in electromagnetic field of near-atomic strength, *Journal of Russian Laser Research* 29(3): 203–218.

Andreev, A. V.; Stremoukhov, S. Yu. & Shoutova, O. A.(2010). Ionization of a multilevel atom by ultrashort laser pulses, *Zh. Eksp. Teor. Fiz.* 111(6): 936Ű948.

Bartel, T.; Gaa, P.; Reimann, K.; Woerner, M. & Elsaesser, T.(2005). Generation of single-cycle thz transients with high electric-field amplitudes, *Optics Letters* 30(20): 2805–2807.

Bauer, D. & Koval, P. (2006). Qprop: A schrodinger-solver for intense laser-atom interaction, *Comp. Phys. Comm.* 174(5): 396–421.

Bauer, D.; Milosevic, D. B. & Becker, W.(2005). Strong-field approximation for intense-laserŰatom processes: The choice of gauge, *Phys. Rev. A* 72: 023415.

Cook, D. J. & Hochstrasser, R. M. (2000). Intense terahertz pulses by four-wave rectification in air, *Optics Letters* 25(16): 1210–1212.

Corkum, P. B. & Krausz, F. (2007). Attosecond science, *Nature Physics* 3: 381–387.

Corkum, P. B.; Burnett, N. H. & Ivanov, M. Y.(1994). Subfemtosecond pulses, *Optics Letters* 19 (22): 1870–1872.

Faisal, F. H. M. (1973). Multiple absorption of laser photons by atoms, *J. Phys. B: At. Mol. Phys.* 6: L89.

Ganeev, R. (2009). Generation of high-order harmonics of high-power lasers in plasmas produced under irradiation of solid target surfaces by a prepulse, *Phys. Usp* 52: 55–77.

Ganeev, R. A.; Baba, M.; Suzuki, M. & Kuroda, H.(2005). High-order harmonic generation from silver plasma, *Phys. Lett. A* 339: 103–109.

Ganeev, R. A.; Elouga Bom, L. B.; Kieffer, J.-C.; Suzuki, M.; Kuroda, H. & Ozaki, T.(2007a). Demonstration of the 101st harmonic generated from a laser-produced manganese plasma, *Phys. Rev. A* 76: 023831.

Ganeev, R.A.; Singhal, H.; Naik, P.A.; Chakravarty, U.; Arora, V.; Chakera, J.A.; Khan, R.A.; Raghuramaiah, M.; Kumbhare, S.R.; Kushwaha, R.P. & Gupta, P.D. (2007b). Optimization of the high-order harmonics generated from silver plasma, *Applied Physics B: Lasers and Optics* 87(2): 243–247.

Gorbunov, L. M. & Frolov, A. A. (1996). Emission of low-frequency electromagnetic waves by a short laser pulse in stratified rarefied plasma, *JETP* 83(5): 967.

Hamster, H.; Sullivan, A.; Gordon, S.& Falcone, R. W.(1994). Short-pulse terahertz radiation from high-intensity-laser-produced plasmas, *Phys. Rev. E* 49: 671Ű677.

Hamster, H.; Sullivan, A.; Gordon, S.; White, W. & Falcone, R. W.(1993). Subpicosecond, electromagnetic pulses from intense laser-plasma interaction, *Phys. Rev. Lett.* 71: 2725Ű2728.

Itatani, J.; Levesque, J.; Zeidler, D.; Niikura, H.; Pepin, H.; Kieffer, J. C.; Corkum, P. B. & Villeneuve, D. M. (2004). Tomographic imaging of molecular orbitals, *Nature (London)* 432: 867Ű871.

Keldysh, L.V. (1965). Ionization in the field of a strong electromagnetic wave, *Sov. Phys. JETP* 20: 1307.

Kim,K.Y.; Taylor,A.J.; Glownia,A.J. & Rodriguez, G.(2008). Coherent control of terahertz supercontinuum generation in ultrafast laser-gas interactions, *Nature photonics* 2: 605–609.

Krause, J. L.; Schafer, K. J. & Kulander, K. C.(1992). High-order harmonic generation from atoms and ions in the high intensity regime, *Phys. Rev. Lett.* 68: 3535Ű3538.

Kress, M.; Loffler, T.; Eden S.; Thomson, M. & Roskos, H. G.(2004). Terahertz-pulse generation by photoionization of air with laser pulses composed of both fundamental and second-harmonic waves, *Optics Letters* 29(10): 1120–1122.

Kulander, K. C.; Schafer, K. J. & Krause, J. L.(1991). Dynamic stabilization of hydrogen in an intense, high-frequency, pulsed laser field, *Phys. Rev. Lett.* 66: 2601Ű2604.

Landau, L. D. & Lifshits, E. M. (1981). *Quantum Mechanics, 3rd ed.*, Elsevier Science.

Marte, P. & Zoller, P. (1991). Hydrogen in intense laser fields: Radiative close-coupling equations and quantum-defect parametrization, *Phys. Rev. A* 43: 1512Ű1522.

Muller, H. (1999). An efficient propagation scheme for the timedependent schrodinger equation in the velocity gauge, *Laser Phys.* 9: 138.

Papadogiannis, A.; Nikolopoulos, L.A.A.; Charalambidis, D.; Tzallas, P.;Tsakiris, G. & Witte, K.(2003). Two xuv-photon ionization of he through a superposition of higher harmonics, *Phys. Rev. Lett* 90: 133902.

Parker, J. & Stroud, C. R. (1990). Population trapping in short-pulse laser ionization, *Phys. Rev A* 41(3): 1602.

Paul, P. M.; Toma, E. S.; Breger, P.; Mullot, G.; Aug, F.; Balcou, Ph.; Muller, H. G. & Agostini, P. (2001). Observation of a train of attosecond pulses from high harmonic generation, *Science* 292: 1689.

Perelomov, A. M. & Popov, V. S. (1967a). Ionization of atoms in alternating electric field. iii, *Sov. Phys. JETP* 25: 336–343.

Perelomov, A.M.; Popov, V.S. & Terent'ev, M.V. (1967b). Ionization of atoms in an alternating electric field, *Sov. Phys. JETP* 24: 207.

Pont, M. & Gavrila, M. (1990). Stabilization of atomic hydrogen in superintense, high-frequency laser fields of circular polarization, *Phys. Rev. Lett.* 65: 2362Ű2365.

Popov, V. S. (2004). Tunnel and multiphoton ionization of atoms and ions in a strong laser field (keldysh theory), *Phys. Usp.* 47: 47 855Ű885.

Popov, V. S.; Kuznetsov, V. P. & Perelomov, A. M.(1968). *Sov. Phys. JETP* 26: 222.

Rae, S.C.; Chen, X. & Burnett, K.(1994). Saturation of harmonic generation in one- and three-dimensional atoms, *Phys. Rev. A* 50: 1946–1949.

Redkin, P. V. & Ganeev, R. A. (2010). Simulation of resonant high-order harmonic generation in a three-dimensional fullerenelike system by means of a multiconfigurational time-dependent hartree-fock approach, *Phys. Rev. A* 81: 063825.

Reiss, H. R. (1990). Complete keldysh theory and its limiting cases, *Physical Review A* 42 (3): 1476–1486.

Reiss, H. R. (1992). Theoretical methods in quantum optics: S-matrix and keldysh techniques for strong-field. processes, *Prog. Quantum Electron* 16: 1.

Reiss, H. R. (1980). Effect of an intense electromagnetic field on a weakly bound system, *Phys. Rev. A* 22: 1786Ű1813.

Sola, I. J.; Melvel, E.; Elouga, L.; Constant, E.; Strelkov, V.; Poletto, L.; Villoresi, P.; Benedetti, E.; Caumes, J.-P.; Stagira, S.; Vozzi, C.; Sansone, G. & Nisoli, M.(2006). Controlling attosecond electron dynamics by phase-stabilized polarization gating, *Nature Physics* 2: 319 – 322.

Sprangle, P.; Peano, J. R.; Hafizi, B. & Kapetanakos, C. A.(2004). Ultrashort laser pulses and electromagnetic pulse generation in air and on dielectric surfaces, *Phys. Rev. E* 69: 066415.

Suzuki, M.; Baba, M.; Kuroda, H.; Ganeev, R. A. & Ozaki, T.(2007). Intense exact resonance enhancement of single-high-harmonic from an antimony ion by using ti:sapphire laser at 37 nm, *Optics Express* 15(3): 1161–1166.

Tobey, R. I.; Siemens, M. E.; Cohen, O.; Murnane, M. M. & Kapteyn, H. C.(2007). Ultrafast extreme ultraviolet holography: Dynamic monitoring of surface deformation, *Opt. Lett.* 32: 286.

Volkova, E. A.; Gridchin, V. V.; Popov, A. M. & Tikhonova, O. V.(2006). Tunneling ionization of a hydrogen atom in short and ultrashort laser pulses, *Journal of Experimental and Theoretical Physics* 102(1): 40–52.

Volkova, E. A.; Popov, A. M. & Tikhonova, O. V. (2001). Ionization and stabilization of a three-dimensional system with a short-range potential in a strong laser field, *Journal of Experimental and Theoretical Physics* 93(6): 1155–1162.

Volkova, E. A.; Popov, A. M.; Tikhonov, M. A. & Tikhonova, O. V.(2007). Atom under an intense laser pulse: Stabilization effect and strong-field approximation, *Journal of Experimental and Theoretical Physics* 105(3): 526–534.

Watanabe, S.; Kondo, K.; Nabekawa, Y.; Sagisaka, A. & Kobayashi, Y.(1994). Two-color phase control in tunneling ionization and harmonic generation by a strong laser field and its third harmonic, *Phys. Rev. Lett.* 73: 2692Ű2695.

Yin, Y.-Y.; Chen, C.; Elliott, D. S. & Smith, A. V.(1992). Asymmetric photoelectron angular distributions from interfering photoionization processes, *Phys. Rev. Lett.* 69: 2353Ű2356.

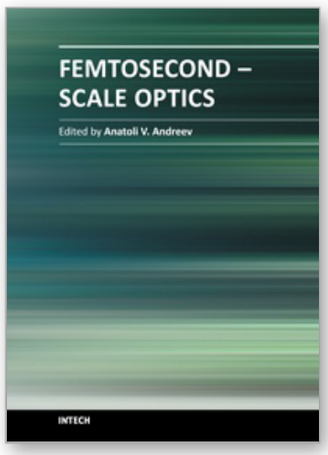

Femtosecond-Scale Optics
Edited by Prof. Anatoly Andreev

ISBN 978-953-307-769-7
Hard cover, 434 pages
Publisher InTech
Published online 14, November, 2011
Published in print edition November, 2011

With progress in ultrashort ultraintense laser technologies the peak power of a laser pulse increases year by year. These new instruments accessible to a large community of researchers revolutionized experiments in nonlinear optics because when laser pulse intensity exceeds or even approaches intra-atomic field strength the new physical picture of light-matter interaction appears. Laser radiation is efficiently transformed into fluxes of charged or neutral particles and the very wide band of electromagnetic emission (from THz up to x-rays) is observed. The traditional phenomena of nonlinear optics as harmonic generation, self-focusing, ionization, etc, demonstrate the drastically different dependency on the laser pulse intensity in contrast the well known rules. This field of researches is in rapid progress now. The presented papers provide a description of recent developments and original results obtained by authors in some specific areas of this very wide scientific field. We hope that the Volume will be of interest for those specialized in the subject of laser-matter interactions.

How to reference
In order to correctly reference this scholarly work, feel free to copy and paste the following:

A.V. Andreev, S.Yu. Stremoukhov and O.A.Shoutova (2011). Interaction of Atom With Laser Pulses of Intra-Atomic Field Strength, Femtosecond-Scale Optics, Prof. Anatoly Andreev (Ed.), ISBN: 978-953-307-769-7, InTech, Available from: http://www.intechopen.com/books/femtosecond-scale-optics/interaction-of-atom-with-laser-pulses-of-intra-atomic-field-strength

INTECH
open science | open minds

InTech Europe
University Campus STeP Ri
Slavka Krautzeka 83/A
51000 Rijeka, Croatia
Phone: +385 (51) 770 447
Fax: +385 (51) 686 166
www.intechopen.com

InTech China
Unit 405, Office Block, Hotel Equatorial Shanghai
No.65, Yan An Road (West), Shanghai, 200040, China
中国上海市延安西路65号上海国际贵都大饭店办公楼405单元
Phone: +86-21-62489820
Fax: +86-21-62489821

IntechOpen